SENSING VEGETATION GROWTH AND SENESCENCE WITH REFLECTED GPS SIGNALS: ACTIVE MICROWAVE DETECTION OF WESTERN NORTH AMERICA PHENOLOGY

by

Sarah Grace Evans

B.A., Whitman College, 2011

A thesis submitted to the

Faculty of the Graduate School of the

University of Colorado in partial fulfillment

of the requirement for the degree of

Master of Science

Department of Geological Science

2013

This thesis entitled:
Sensing vegetation growth and senescence with reflected GPS signals:
Active microwave detection of western North America phenology
written by Sarah Grace Evans
has been approved for the Department of Geological Sciences

_____
Eric Small Tilton, Committee Chair

_____
Kristine Larson, Committee Member

_____
John Braun, Committee Member

Date_____

The final copy of this thesis has been examined by the signatories, and we find that both the content and the form meet acceptable presentation standards of scholarly work in the above mentioned discipline.

Evans, Sarah Grace (M.S., Geological Sciences)

Sensing Vegetation Growth and Senescence with Reflected GPS Signals:

Active Microwave Detection of Western North America Phenology

Thesis directed by Associate Professor Eric Small Tilton

We explore a new technique to estimate vegetation growth and senescence using reflected GPS signals (multipath) measured by geodetic-quality GPS stations. The operational GPS-IR statistic Normalized Microwave Reflection Index (NMRI), a measure of multipath scattering, exhibits a clear seasonal cycle as is expected for vegetation growth and senescence. The sensing footprint is ~1000 m^2, larger than that provided by typical *in situ* observations but smaller than that from space-based products. Since GPS satellites transmit L-band signals, the vegetation estimates derived from GPS reflections provide global phenology monitoring that is sensitive to changes in vegetation canopy water content and biomass. However, GPS reflections are insensitive to plant greenness, clouds, atmosphere, and solar illumination constraints that adversely affect optical-infrared remote sensing vegetation indices like Normalized Difference Vegetation Index (NDVI).

Temporal and spatial diffuse scattering of microwave GPS-IR index NMRI and MODIS-based NDVI is documented at both the site-by-site and regional scale at 184 sites over the western United States. We derive NMRI and NDVI range, correlation between NMRI and NDVI signals, and phenology parameters including: start of season, season length, and peak day of year of vegetation growth. These phenology indexes are compared over a five water-year time series (2008 to 2012) to gauge spatial and temporal offsets. Average correlations (R^2=0.527) were found with NMRI variations lagging NDVI by approximately 21 days. This is consistent with the idea that greenup precedes plant growth. Phenology metrics extracted by microwave NMRI record a later start of season, later peak day of year, and shorter season length than determined by optical NDVI. Metrics are offset spatially with the largest offsets along Pacific Ocean coastline, decreasing inland and subdivided by region, supporting that plant growth cycles are controlled by regional climates. This study is the first attempt to validate and compare GPS network derived reflectance index with optical-infrared remote sensing index NDVI, and highlights both opportunities and limitations offered by NMRI data.

Acknowledgements

I acknowledge funding from NSF EAR-0948957, NSF AGS-0935725, and NASA NNH09ZDA001N. Many GPS results are based on data, equipment, and engineering services provided by the Plate Boundary Observatory operated by UNAVCO for EarthScope and supported by NSF (EAR-0350028 and EAR-0732947).

I thank my advisor, Eric Small Tilton, for his patience, encouragement, and guidance through my time at The University of Colorado. Without him this thesis would not have been possible. I also thank Kristine Larson and all members past and present of the GPS Reflections Group at CU for their continued feedback and assistance.

Thank you to my fellow graduate students for their support intellectually and emotionally. In particular I thank Shahen Huda, Cailey Condit, Nadine Reitman, Billy Armstrong, Clara Chew, Aidan Beers, and Peter Shellito for keeping my spirits up, teaching me how to code, laughing with and at me, getting me outside, and generally being wonderful friends. Diane Feuillet has been the source of continued laughs and unwavering support from afar.

Finally, I offer special thanks to my parents and brother for the inspiration, love, encouragement, and many great (bad?) puns they have always offered. "You got a point there, but if you put on a cap no one will notice".

Contents

Chapter

1. INTRODUCTION 1
    1.1 Motivation 1
    1.2 Optical remote sensing 2
    1.3 Microwave remote sensing 3
    1.4 Benefits of GPS-IR 4
    1.5 Purpose of this study 6

2. DERIVATION OF NMRI AND NDVI METRICS 8
    2.1 Data acquisition 8
        2.1.a MP1rms 8
        2.1.b NDVI 10
        2.1.c Precipitation and temperature 10
    2.2 Data cleaning 11
    2.3 Range, correlation, and lag metric derivation 12
    2.4 NMRI and NDVI seasonality metric derivation 12
        2.4.a Smoothing NMRI and NDVI 13
        2.4.b Phenology variables 13
        2.4.c Uncertainty and sensitivity to parameters 15
    2.5 North America level III/IV ecoregions 16

3. RESULTS 18
    3.1 NMRI and NDVI range 18
        3.1.a Range values 18
        3.1.b Spatial trends 19
    3.2 Correlation between NDVI and NMRI 21
        3.2.a Site-by-site correlation 21
        3.2.b Correlation by region 22
        3.2.c Lag effects and correlation 23

3.3 Relationship between NMRI and NDVI phenology metrics 26
3.3.a Phenology metrics: Five water-year time series 26
3.3.b 2012 drought variability 30
3.3.c 2012 drought results 31
3.4 NMRI and NDVI metrics as a function of climatic variables 32
3.4.a Mean Annual Temperature 32
3.4.b Mean Annual Precipitation 34
3.4.c Latitude 34

4. DISCUSSION 36
4.1 NMRI constrains and bias 36
4.1.a Temperature-limited regions 36
4.1.b Precipitation-limited regions 37
4.1.c Insolation-limited regions 39
4.2 Drought 40

5. CONCLUSIONS 43

BIBLIOGRAPHY 44

Tables

Table

1. NMRI and NDVI parameters separated by region 18

2. Phenology metrics.....27

3. Seasonality parameters for 2012 v. 2008-2012 average 31

4. Phenology R^2 and p-values 34

Figures

Figure

1. Photographs of site p208 5
2. NMRI and NDVI seasonality metric derivation 14
3. Map of sites and ecoregions 16
4. Map of NMRI and NDVI ranges 19
5. Plot of range with site averages 20
6. R^2 by month for sites p022, p041, and p208 21
7. Box and whisker plot of R^2 with histogram of lag days 23
8. Map of lag week and R^2 values 24
9. Histogram of lab days by region 25
10. Start of season and peak vegetation day of year (doy) by region 26
11. Maps of start of season and peak vegetation doy for NDVI and NMRI 29
12. Drought effect on sites p208, p042, and p048 30
13. NDVI and NMRI seasonality metric by climatic variables 33
14. NMRI and NDVI signals for site p398 40
15. Map of drought extent in 2012 41

CHAPTER 1

Introduction

1.1 Motivation

Vegetation state measurements are necessary for monitoring the phenology of ecosystem variables (Rondeaux et al., 1996; White et al., 2009; Jones et al., 2011), validating long-term land cover satellite estimates (Lu, 2006; Hobbs et al., 2007), and testing climate change and carbon cycle models (Cihlar et al., 1991; Sellers et al., 1992; Paruelo & Aguiar, 1993; Sellers et al., 1995; Nemani et al., 2003). With increasing temperatures and amplified drought conditions expected in the long term (Karl et al., 2012) it is becoming necessary for ecohydrologists to understand how water is used by vegetation before characterizing climatic and soil-water interactions at regional and even global areas (Burke et al., 1991; Paruelo & Lauenroth, 1995; Rodriguez-Iturbe, 2000).

Phenology, the study of the timing of biological events, integrates climate-biosphere relationships and is used to evaluate the effects of climate change (Schwartz et al., 2006; Cleland et al., 2007). Understanding the timing, rate, and duration of vegetation growth events is key in the study of global change and the carbon cycle. This timing relates directly to vegetation photosynthesis, carbon sequestration, and land–atmosphere water and energy exchange (Peñuelas, 2009; Morisette et al., 2009; Jones et al., 2011). Variations in seasonal onset of vegetation growth have been documented at both the *in situ* measurement scale (Wolfe et al., 2005) and the global satellite derived scale (Karl et al., 2012). With recent climate change, phenologists have noted earlier spring onset and delays in the end of growing seasons (Parmesan, 2007; Peñuelas, 2009). In order to advance precise vegetation measurements, we need new

methods to remotely sense vegetation and derive phenology metrics at appropriate spatial and temporal scales.

1.2 Optical remote sensing

Normalized Difference Vegetation Index (NDVI), one of the most widely used vegetation remote sensing methods, is calculated as the difference between near-infrared (NIR) and visible (VIS) reflectance values normalized over the sum of the two (Eidenshink, 1992):

$$\mathrm{NDVI} = \frac{(\mathrm{NIR} - \mathrm{VIS})}{(\mathrm{NIR} + \mathrm{VIS})}$$

Healthy green leaves have an internal mesophyll structure that reflects near-infrared radiation and also contain leaf chlorophyll to absorb red visible radiation (Wang et al., 2003). This makes NDVI a good indicator of the ability of plant matter to absorb photosynthetically active radiation. Therefore, NDVI is often used to estimate green biomass or phytomass (Gamon et al., 2012; Al-Bakri and Taylor, 2003; Holm, 2003), leaf area index (Burke et al., 1991; Goetz, 1997), evapotranspiration (Cihlar et al., 1991), and primary productivity (Box et al., 1989; Rodriguez-Iturbe, 2000; Paruelo et al., 1997). For over 30 years, NDVI has provided direct measures of the phenological state of vegetation from landscape to global scales (Tarpley et al., 1984; Running & Nemani, 1988).

While NDVI is documented as a successful "greenup" and seasonality index, it still has a variety of shortcomings: it has problems with background effects from soil (Paruelo et al., 1997), atmospheric effects (Rondeaux et al., 1996; Myneni & Williams, 1994), smoke and aerosol contamination (Jones et al., 2011), cloud cover (Champion and Guyot, 1993), areas of complex terrain (Box et al., 1989), weather (Brakke et al., 1981), time of day (Kim et al., 2012), and interruption of signals at high latitudes (Box et al., 1989). Accurate derivation of phenology

metrics, such as vegetation start of season, suffer from the coarse time step of NDVI (Fischer, 1994). Additionally, NDVI has limited sensitivity to drought conditions due to its spatial compositing procedure which biases the high end of its spectral signature (Burke et al., 1991). As global phenology patterns and trends shift with climate change (Jones et al., 2011), dry conditions may become exacerbated (Enquist et al., 2012), increasing this problem.

Other spectral vegetation indices such as Soil-Adjusted Vegetation Indices (SAVI) include soil-line parameters (Rondeaux et al., 1996). Compared to NDVI, SAVI considerably reduces soil influences and surface roughness resulting in a lowered vegetation index signal (Huete, 1988). Although SAVI reduces soil effects, it still has imprecise vegetation estimates, particularly when there is low vegetation cover (Rondeaux et al., 1996). SAVI is not as commonly used as NDVI. Normalized Difference Water Index (NDWI), another optical remote sensing method, utilizes an absorption band at 1.24 μm, whereas NDVI uses a channel at 0.66 μm. NDWI measures interactions between liquid water molecules in vegetation canopies and incoming solar radiation (Chen et al., 2005). However, NDWI is not a better predictor of vegetation water content than NDVI, especially at sites with soil background reflectance effects (Gao, 1996). Therefore, only NDVI will be addressed further as a comparison index.

1.3 Microwave remote sensing

Remote sensing with microwave radar has advantages in that it is not limited by cloud cover, weather, or time of day (Ulaby & Wilson, 1985). There are two types of microwave remote sensing: active and passive. While active microwave sensing receives backscattering reflections from transmitted microwave signals on a plane, satellite, or ground surface, passive

microwave sensing gathers microwave radiation emitted directly from objects on the ground (Murai, 1993).

Microwave data may be used to accurately determine vegetation water content and estimate biomass (Lu, 2006; Kim et al., 2012). As the dielectric constant for water is an order of magnitude greater than for dry soil or vegetation at microwave wavelengths (Schmugge, 1978), changes in moisture content can results in significant changes in microwave scattering coefficients (Brakke et al., 1981). Thus, the primary challenges when using microwave data for vegetation studies include integrating heterogeneous plant dielectric properties through the canopy layer (O'Neill et al., 1984), and removing the effects of soil moisture and surface roughness (De Roo et al., 2001; Ulaby & Wilson, 1985; Ulaby et al., 1984).

1.4 Benefits of GPS-IR

Global Positioning System-Interferometric Reflectometry (GPS-IR), an active bistatic radar remote sensing technique, has shown great potential as a continuous, all-weather, and close to real-time microwave radar system for monitoring biomass (Small et al., 2010; Jin et al., 2011). GPS satellites transmit L-band (microwave bands at 1.22760 and 1.57542 GHz) signals similar to those used in active microwave radar applications. L-band signals have a higher correlation with vegetation water content (Kim et al., 2012) than C-band signals (4 to 8 GHz). GPS-IR instruments can retrieve snow depth (Larson et al., 2009; Larson and Nievinski, 2012), soil moisture content (Larson et al., 2010) and even vegetation state (Hawkes and Finn, 2000; Small et al., 2010; Rodriguez-Alvarez et al., 2011). Since GPS satellites transmit L-band signals, the vegetation estimates derived from GPS reflections are a measure of vegetation water content, not greenness as is the case for optical remote sensing methods.

GPS-IR is able to measure surface environmental variables through multipath delay, one of the main error sources for GPS navigation and positioning (Jin and Komjathy, 2010). Multipath delay arises through interactions between the reflected ground signal and direct signal transmitted from the satellite to the antenna. Geodetic GPS instruments optimized to track direct satellite signals and suppress multipath signals may be used to measure reflected signals (Larson et al., 2008). These geodetic GPS (Fig. 1) systems, such as the tens of thousands worldwide and ~1000 currently operating under the National Science Foundation (NSF) EarthScope Plate Boundary Observatory (PBO), can be utilized to estimate biophysical parameters through multipath amplitude variations. The majority of PBO sites are located in the western United States along active plate margins to measure deformation of the Pacific-North America plate boundary. Thus the highest density of sites is in California. Vegetation types at PBO sites are dominantly grass, woody savanna, and shrub.

Figure 1. GPS antenna and radome in the foreground at site p208 in Williams, California. This site was visited in 2012 to verify NMRI results. On the top is lush green oatgrass on April 14th, 2012. On the bottom is the same site three months later on July 22nd, 2012 with dry, brown vegetation.

GPS-IR has many benefits over other remote sensing techniques of vegetation sampling. The sensing footprint of GPS (~1000 m^2) is smaller than that of spaced-derived remotely sensed products such as spectral vegetation indices (~25,000 m^2), but larger than that of *in situ* observations (e.g. clipping and drying, ~1 m^2). Additionally, GPS instruments can provide daily estimates of vegetation state (Jones et al., 2011), which is more frequent than the, at best, four day composites of other sensing devices like NDVI (Jones et al., 2012).

The operational GPS-IR statistic MP1rms, a measure of multipath scattering, exhibits a clear seasonal cycle as is expected for vegetation growth and senescence. MP1rms is the root mean square of a linear combination of L1 and L2 carrier phase data with L1 pseudorange data (Estey and Meertens, 1999). Normalized Microwave Reflection Index (NMRI) is the normalized version of MP1rms with a reverse in sign so that it increases during the growing season. This normalization is discussed in more details in Section 2.

1.5 Purpose of this study

While the correlation between NMRI and vegetation has already been suggested (Small et al., 2010), the relationship between NMRI and NDVI signals needs further quantification. The purpose of this study is to compare NMRI and NDVI signals spatially in terms of temporal signal variation and phenology. We derive NMRI and NDVI range, correlation between NMRI and NDVI signals, and phenology parameters at both the site-by-site and regional scale for the western United States. Phenology metrics include start of season day of year, season length, and peak day of year of vegetation growth. The primary objectives of this study were to: 1) use range, correlation, and timing of phenology metrics to quantify spatial changes between NDVI and NMRI indexes, 2) measure temporal phenology changes between NMRI and NDVI for an

averaged five year record versus a drought year (2012), and 3) examine phenology variables as a function of climatic constrains including precipitation, temperature, and latitude.

CHAPTER 2

Derivation of NMRI and NDVI metrics

190 sites from the NSF PBO Network in the western United States were initially chosen. Sites were selected in California, Oregon, Montana, Nevada, Utah, Idaho, Wyoming, and Colorado in non-forested, non-urbanized areas without seasonal snowpack. Data from all sites was processed uniformly. Through data acquisition and cleaning processes, described below, the number of study sites was reduced to 184.

2.1 Data acquisition

2.1.a MP1rms

Originally GPS was designed as a two-frequency system: L1 and L2 which operate at 1.57542 and 1.22760 GHz, respectively. Both of these frequencies consist of pseudorange data and carrier phase data. Pseudorange data are a measurement of the time shift required to line up generated receiver code with code received from satellite multiplied by the speed of light (Wells et al., 1999). Carrier phase data are the phase of the signal that remains when the incoming carrier is differenced with the constant frequency generated by the receiver (Wells et al., 1999). Pseudorange data (P) equals:

$$P_{1_r}^{\ s} = p_r^s + c\delta_r - c\delta^s + T + \frac{I}{{f_1}^2} + M_1 + \mathcal{E}_1$$

$$P_{2_r}^{\ s} = p_r^s + c\delta_r - c\delta^s + T + \frac{I}{{f_2}^2} + M_2 + \mathcal{E}_2$$

Where P_1 is the observed pseudorange on the L1 frequency (1.57542 GHz) and P_2 is the observed pseudorange on the L2 frequency (1.22760 GHz) for a given receiver (r) and satellite (s). A GPS receiver measures how long it thinks it took the signal to travel from the satellite to

the antenna, and multiplies this by c, the speed of light. Atmospheric delays are represented by T (troposphere) and I (ionosphere), where the dependence on both the receiver and satellite is assumed. The geometric range (p_r^s) represents the path traveled by the satellite signal in a vacuum between the satellite and the antenna, δ represents clock errors for either the receiver or satellite. Mulipath is represented by the M term. $\mathcal{E}$ is the intrinsic measurement error due to the ability of the GPS receiver to track the signal. Carrier phase (ϕ) data equals:

$$\lambda_1 \phi_{1_r^s} = p_r^s + c\delta_r - c\delta^s + T - \frac{I}{{f_1}^2} + N_1\lambda_1 + \mathcal{E}_{\phi 1}$$

$$\lambda_2 \phi_{2_r^s} = p_r^s + c\delta_r - c\delta^s + T - \frac{I}{{f_2}^2} + N_2\lambda_2 + \mathcal{E}_{\phi 2}$$

With the carrier phases (for the two frequencies) represented by ϕ_1 and ϕ_2. λ_1 and λ_2 are the GPS L1 and L2 wavelengths (~0.19 and 0.244 m). N_1 and N_2 represent integer phase ambiguities. These uncertainties should be constant throughout a satellite arc so long as there are no cycle slips.

Since the wavelength of the carrier phase is much shorter than the wavelength of either codes, carrier phase codes have much greater precision than pseudo-range codes (Wells et al., 1999). M_1 or multipath error on pseudorange data are of interest in this study as it is two orders of magnitude larger than carrier phase multipath errors. MP_1 may be isolated by subtracting pseudorange data from carrier phase data producing the following linear combination:

$$MP_1 = P_1 - \frac{{f_1}^2 + {f_2}^2}{{f_1}^2 - {f_2}^2}\lambda_1\phi_1 + \frac{{f_1}^2 + {f_2}^2}{{f_1}^2 - {f_2}^2}\lambda_2\phi_2$$

This removes the geometrics range and clocks simplifying to:

$$MP_1 = M_1 + \mathcal{E}_1 + C$$

Here C is a linear combination of the carrier phase bias terms. MP_1 can be estimated when all three GPS observables (P_1, ϕ_1, ϕ_2) are known. To avoid error, slips that could vary N_1 and N_2 values must be identified and repaired.

Thus, MP1rms is the root mean square of a linear combination of L1 and L2 carrier phase data with L1 pseudorange data (Estey and Meertens, 1999). Every day, MP1 is recorded from each GPS antenna in the PBO network for every satellite that passes overhead at a sampling interval of 15 seconds. A constant is then removed; standard deviations are computed from these values, and ultimately averaged, producing one daily MP1rms value for each site. MP1rms is unitless.

2.1.b NDVI

NDVI data are derived from NASA's Moderate Resolution Imaging Spectroradiometer (MODIS), MOD13Q1, 250 meter pixel, 16-day composite products. 250 meter spatial resolution is used because the 250 meter bands detect light in the near infrared and red portions of the electromagnetic spectrum. Each NDVI data point is a composite created using the Maximum Value Composite (MVC) technique. This technique is frequently performed on NDVI data to reduce both cloud contamination and data volume (Swets et al., 2001). Using the MVC technique, points with the highest NDVI from daily images over 16-day periods are selected and reported (Holm, 2003). For this study, data points are extracted and averaged from one pixel surrounding a stationary centroid of each sampling domain. NDVI is unitless.

2.1.c Precipitation and temperature

Mean annual precipitation (MAP, mm) and mean annual temperature (MAT, ºC) are extracted from hourly North America Land Data Assimilation System (NLDAS-2) modeled data at each site (Mitchell et al., 2003). Daily values are computed (maximum, minimum, and

average) for each of these quantities. This data has 32 km spatial resolution and one hour temporal frequency (NLDAS; http://ldas.gsfc.nasa.gov/nldas/NLDAS2model.php).

2.2 Data cleaning

NDVI is minimally edited. Negative NDVI values are set to zero and data are removed on days that NLDAS data record snow events. NLDAS snow events are identified when the temperature falls below 1 ºC and there is more than 2 mm of daily precipitation.

MP1rms data are cleaned in the same fashion for NLDAS snow events, but is also cleaned for NLDAS heavy rain events (>10 mm/day) and signal detrending. Since reflected GPS signals are influenced by terrain, and a reflected GPS range signal depends directly on the extra path length, MP1rms metrics have been normalized to become NMRI. At each site, the bare vegetation state is determined empirically by estimating the mean value of data in the top 5th percentile of MP1rms over the six-year period ($MP1_{max}$). Then, with raw MP1rms data defined as $MP1$, NMRI is normalized as follows:

$$NMRI = \frac{-(MP1 - MP1_{max})}{MP1_{max}}$$

Normalizing NMRI this way removes the extra path length term to a first order approximation.

Since NMRI values are influenced by precipitation, soil moisture, surface roughness, and receiver malfunctions, signal noise is variable from site to site. It is challenging to extract metrics at sites with high signal noise. To eliminate these sites, signal noise deviations are determined by computing the standard deviation between the raw NMRI signal and NMRI data after smoothing and linear interpolation. Standard deviations in signal noise range from 0.005 to 0.024 with a mean value of 0.011 (unitless).

Signal noise standard deviations are then compared to the change in NMRI signals, or range, over the six year record (2007-2012). A noise metric picks out sites with high noise standard deviations and low range values; these sites are labeled as "noisy". Noisy sites (n=6) were excluded from metric analysis reducing the number for sites from 190 to 184.

2.3 Range, correlation, and lag metric derivation

After NMRI and NDVI data cleaning and normalization, three metrics are derived on both a site by site (n=184) and region average scale: range, correlation between NMRI and NDVI data, and correlation lag. Range is calculated for NMRI and NDVI for each site as the difference between maximum and minimum data values over the entire data set (2007-2012). Correlation values are found by extracting NMRI data on days that also have NDVI data and computing a standard R^2 coefficient of determination statistic. To take into account lag between NMRI and NDVI signals, NMRI points are extracted for days that have NDVI data plus a specified lag value (in days). R^2 correlation was computed for each lag amount and compared. Lag was tested from zero to 45 days to determine the amount of lag necessary for maximum correlation. 180 sites had positive lag days; four sites had zero or negative lag days. Lag analysis is not exact, as the NDVI data represents a smoothed ~16 day window.

2.4 NMRI and NDVI seasonality metric derivation

Clean and daily NMRI and NDVI data are needed to compute phenology metrics. This poses as a challenge as raw NDVI data are only available as a 16 day composite, making anywhere between one and 31 days between sample points. Likewise, daily NMRI data can be noisy due to variations unrelated to vegetation. In order to overcome these problems and

produce directly comparable data, the same method, outlined below, is used for both NMRI and NDVI phenology metrics.

2.4.a Smoothing NMRI and NDVI

Metrics for NMRI are produced to be directly comparable to NDVI. Examples of smoothing are presented for site p208 in California which has a large range and low noise and site p041 in Colorado which has smaller range and noisier signal (Fig. 2). First, raw NMRI data (Fig. 2a and e) is smoothed with a moving 5-day median (Fig. 2b and f). Next, data are extracted for days that NDVI data was present on a site-by-site basis (Fig. 2c and g), and using linear curve fitting, interpolated for missing data (Fig. 2d and h). It was found that smoothed NMRI extracted on NDVI days matched closely with smoothed NMRI not extracted on correlated NDVI days. Thus for simplification, results are presented in terms of NMRI, not NMRI extracted from days with NDVI. For direct comparison to NMRI, NDVI data are interpolated between missing points using linear curve fitting.

2.4.b Phenology variables

NMRI phenology metrics are then defined with a threshold method (Fig. 2d and h, green line) that requires the data to remain above a fixed 25% of the seasonal amplitude for a minimum of 40 days (Jones et al., 2012). This threshold method was tested against a third derivative approach from an asymmetric Gaussian fitting routine in TIMESAT (Jönsson and Eklundh, 2004). Whereas TIMESAT requires previous and following year data to pad the current year matric, the threshold approach was not limited by padding and able to compute metrics for five water-years, 2008-2012. Each water-year goes from day of year (doy) 275 of the previous year to doy 274 of the current year (for example, the water-year 2012 goes from doy 275 in 2011 to doy 274 in 2012). Annual NDVI metrics are produced using an identical procedure.

Three phenology variables are considered: start of season (SOS), season length, and peak vegetation doy. The SOS or greenup date signifies the first pulse of greenness or increase in vegetation water content. SOS was determined to be when the NMRI or NDVI variable first crosses the 25% threshold (Fig. 2d and h, green line). As a function of each year's minimum signal, the 25% threshold changes from year to year, constructing a moving boundary (e.g., Stein, 1999).

Though 50% is the most often used threshold, as the increase in greenness is believed to be most rapid at this cutoff, we used 25% as to capture the first growth pulse (De Beurs, 2008).

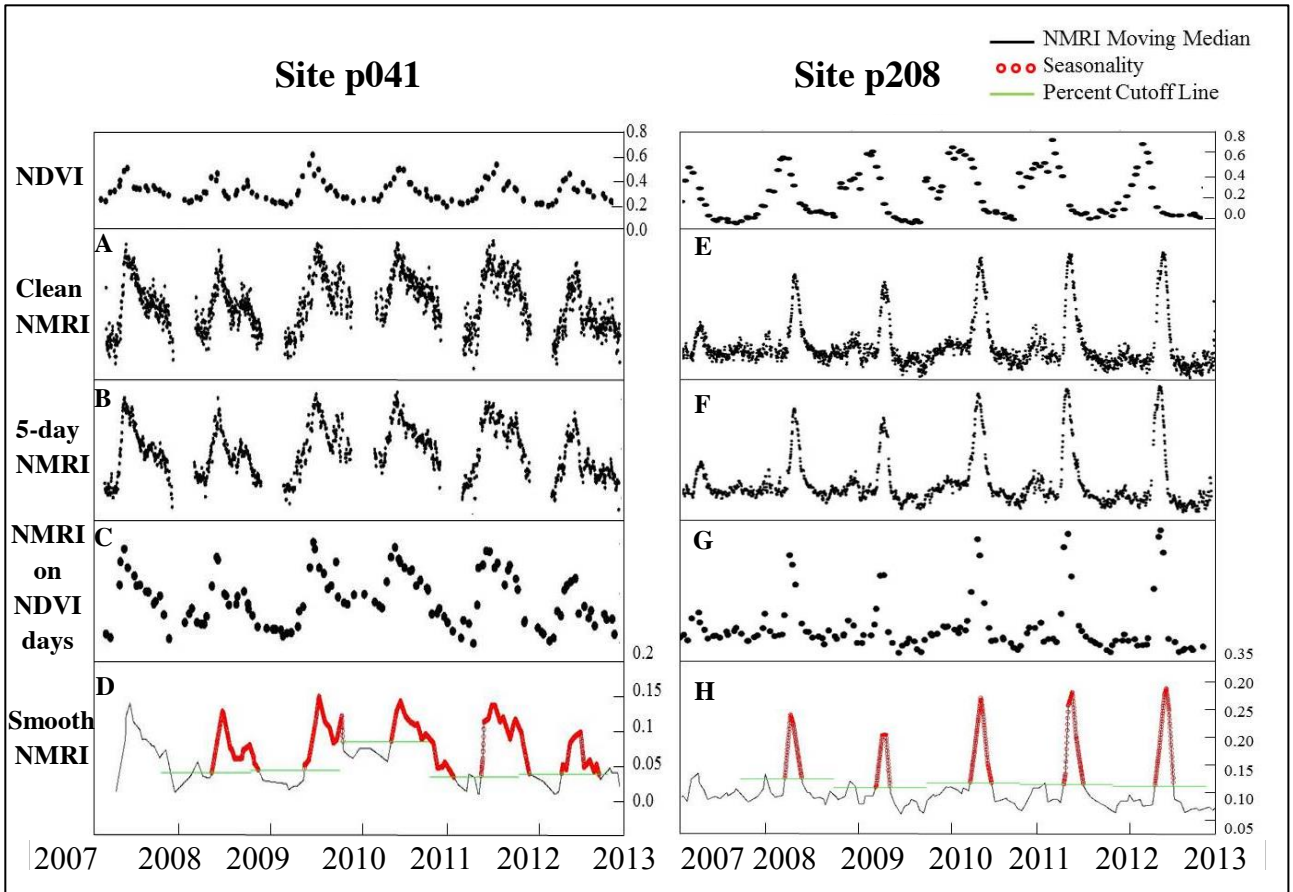

Figure 2. NMRI seasonality metric derivation for sites p041 and p208. Site p041 has a smaller NMRI signal varying from 0-0.1 and has been cleaned for snow while p208 has an uninterrupted record and larger signal range (0-0.3). The red in the bottom panel identifies annual phenology data.

Our criteria also required that the index stay above this percentage for 40 consecutive days (Fig. 2d and h, red dots), as to eliminate any early season increases that may be falsely associated with soil moisture after a heavy precipitation events. Season length (Fig. 2d and h, length of red dots) is computed as the time between SOS and end of season or senescence when the index falls below the 25% threshold. Peak vegetation doy is derived from the doy of the local maximum of the NDVI or NMRI index (Fig. 2d and h, maximum red dot height).

2.4.c Uncertainty and sensitivity to parameters

Six percent of all sites (n=11) were not included for all five water-years for each phenological index due to inadequate extraction of metrics. This occurred when the index did not exceed the 25% threshold for 40 continuous days for the entire year as was often the case at sites with low amplitude variations. Analysis suggests that there is not significant improvement with changes in threshold percent or days above threshold. When computing five water-year averages for the phenological variables, sites were not considered if two or more years had inadequately extracted data, reducing the number of sites analyzed from 184 to 173.

As there is no direct measurement of vegetation biomass at the GPS PBO sites, NMRI and NDVI phenology measurements will only be compared to one another. Any correlation between NMRI and NDVI metrics is not causal and only exists via linkages between plant biomass and water content. We expect that there will be a lag in relations as NMRI is sensitive to the total amount of vegetation water content in the area surrounding the GPS antenna, regardless of the concentration of chlorophyll in the biomass (Small et al., 2010).

2.5 North America level III/IV ecoregions

The Commission for Environmental Cooperation has defined North American level III ecoregions according to climate, hydrology, vegetation, wildlife, and land use/human activities (Wiken et al., 2011). This data set has 181 ecoregions that stretch over the United State, Canada, and Mexico. A further subdivision of level IV ecoregions has been recommended by the U.S. Environmental Protection Agency (Omernik, 1987; U.S. Environmental Protection Agency, 2011). Clustered regional phenology is useful for analyzing phenological responses to climate change on the ecosystem level (White, 2005; Hargrove & Hoffman, 1999).

While this study aims to elucidate ecoregional phenological responses, because of the irregular spacing of test GPS antenna sites (n=184) in the PBO Network, only sites in California, Oregon, Montana, Nevada, Utah, Idaho, Wyoming, and Colorado are

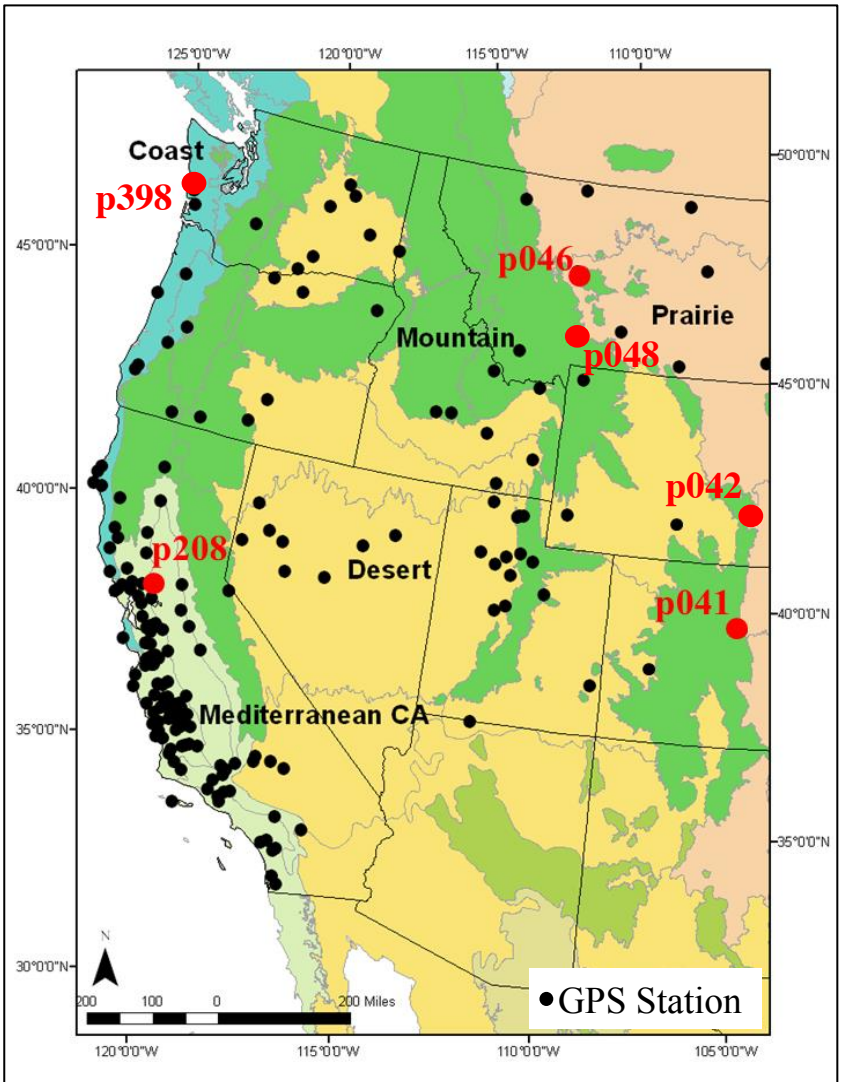

Figure 3. Map showing location of GPS stations used in this study. Six sites of interest are highlighted in red. Ecoregions are identified in black text and color coded.

utilized, spanning 25 level-III ecoregions (Fig. 3). These sub-grouped sites will be referred to by common land-type labels: Mountain (n=25), Coast (n=14), Prairie (n=8), Desert (n=38), and Mediterranean California (n=99). The majority of these stations (n=99) fall into the subdivision of Mediterranean California: California Coastal Sage, Chaparral, and Oak Woodlands. These level III Mediterranean California sites have been subdivided into grassland (n=66) and shrub (n=33) sites based on evaluation of photographs and MODIS land cover classifications. The grassland division contains two cropland sites. By clustering sites into these ecoregions we highlight vegetation phenological responses to climate constraints and reduce the effects of spatial heterogeneity between sites.

CHAPTER 3

Results

3.1 NMRI and NDVI range

3.1.a Range values

Range values highlight the spread of measureable photosynthetic vegetation activity (Reed et al. 1994). NMRI and NDVI range values for each region are reported as a mean of the 2007-2012 data set (Table 1). The average NMRI range value for all sites was 0.25±0.1. The average NDVI range value for all sites was 0.47±0.1. NMRI and NDVI range values should not have equal magnitude as they are normalized independently.

Region Name	Population Size	NMRI Mean Range	NDVI Mean Range	Mean R^2	Max. Mean R^2	Lag Days
Average (2008-2012)	184	0.247±0.09	0.466±0.13	0.310±0.21	0.527±0.20	21±13
Mountain	25	0.216±0.07	0.521±0.10	0.460±0.18	0.606±0.23	9±7
Coast	14	0.170±0.04	0.516±0.16	**0.099±0.14**	**0.280±0.16**	26±16
Prairie	8	0.204±0.04	0.470±0.07	0.492±0.14	0.718±0.07	10±6
Desert	38	0.204±0.07	**0.342±0.13**	0.366±0.21	0.535±0.21	15±9
Med. CA	99	**0.285±0.09**	0.492±0.10	0.261±0.18	0.519±0.17	27±11
Grassland	*66*	*0.315±0.09*	*0.522±0.09*	*0.271±0.17*	*0.543±0.17*	*28±11*
Shrubs	*33*	*0.227±0.07*	*0.437±0.09*	*0.242±0.18*	*0.476±0.15*	*25±12*

Table 1. Mean NMRI and NDVI parameters separated by region. Mediterranean California has been further subdivided into grassland and shrub sites. Outliers identified in bold.

By region, average NMRI and NDVI ranges cluster around the total population mean (Table 3). However, each metric has one regional outlier. For all regions, NDVI ranges are all close to 0.5 except for desert sites that are abnormally low (0.342±0.13). NMRI regional ranges

are all approximately 0.2 with the exception of Mediterranean California sites that have a higher value (0.285±0.09).

3.1.b Spatial trends

Viewed site by site, location appears to have a first-order effect on NMRI and NDVI metric ranges (Fig. 4). NDVI range corresponds differently by region than NMRI range. NMRI range (Fig. 4a) increases with a decrease in latitude while NDVI does not have a consistent pattern (Fig. 4b). The largest NMRI range variations (Fig. 4a, blue points) occur in precipitation-limited Mediterranean California sites (0.29±0.1). Within Mediterranean California the grassland sites have higher mean range (0.32±0.1), with range decreasing towards

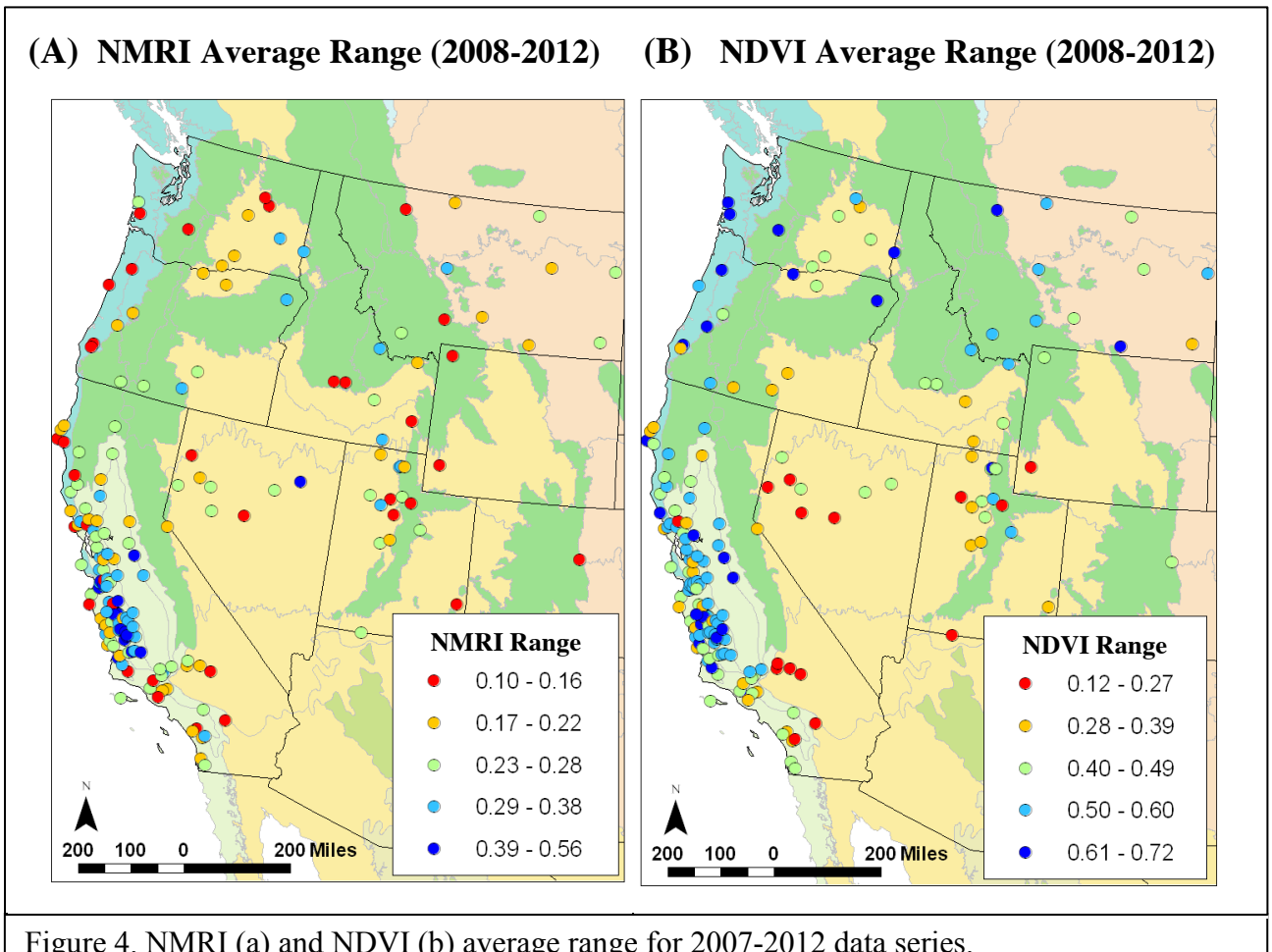

Figure 4. NMRI (a) and NDVI (b) average range for 2007-2012 data series.

the coast. The highest range values cluster around the agricultural Central Valley in California. Mountain sites also have relatively high NMRI range (0.22±0.1). The lowest range values (Fig. 4a, red points) are in water-limited western California and the insolation-limited coasts of western Washington and Oregon (0.17±0.0). Desert areas in Nevada and Utah (Fig. 4a, green points) display intermediate values (0.20±0.1). Overall for NMRI, range values within regions are moderately heterogeneous as all regions have standard deviations below 0.1.

Unlike NMRI, NDVI range does not seem to correspond with latitude (Fig. 4b). The highest NDVI values (Fig. 4b, blue points) occur in mountain and coastal regions (0.52±0.1 and 0.52±0.2, respectively). This is in direct contrast to the low NMRI values in the same region (Fig. 4a, red points). The lowest NDVI values (Fig. 4b, red points) cluster around desert areas (0.34±0.1). Intermediate values (Fig. 4b, green points) are found in the prairie and Mediterranean California sites, with values decreasing towards the coast. However, this pattern is not as dramatically as it was for NMRI. There is greater range heterogeneity within region found by NDVI than for NMRI (standard deviations ≤ 0.16).

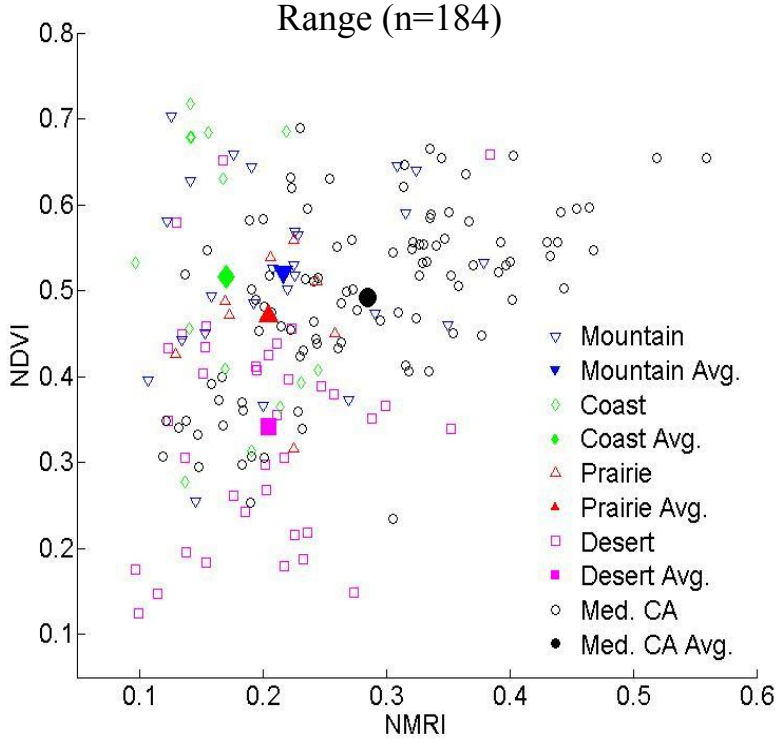

Figure 5. NMRI and NDVI average range for 2007-2012 data series. Each point represents one of 184 sample sites. Filled are averages for each region (see Table 1).

Coast sites have the largest discrepancy between NMRI and NDVI range values. When averaged, this region has the lowest NMRI range value and one of the highest NDVI values (Fig. 5, green diamond). A similar discrepancy is notable in mountain sites (Fig. 5, blue triangle). Since few sites have low NDVI and high NMRI values while many sites have high NDVI and low NMRI values, there is an unequal relationship between NMRI and NDVI ranges that creates a triangular skew in the data as seen in Figure 5.

3.2 Correlation between NDVI and NMRI

3.2.a Site-by-site correlation

We report average data series (2007-2012) R^2 correlation values between NDVI and NMRI signals for each region (Table 1). Three different sites are presented as examples of correlation: p041, p046, and p208 (Fig. 6). At site p041 in Marshall, Colorado (R^2=0.65) the NDVI and NMRI values are not stratified by month (see Figure 2 for time series). Prairie site

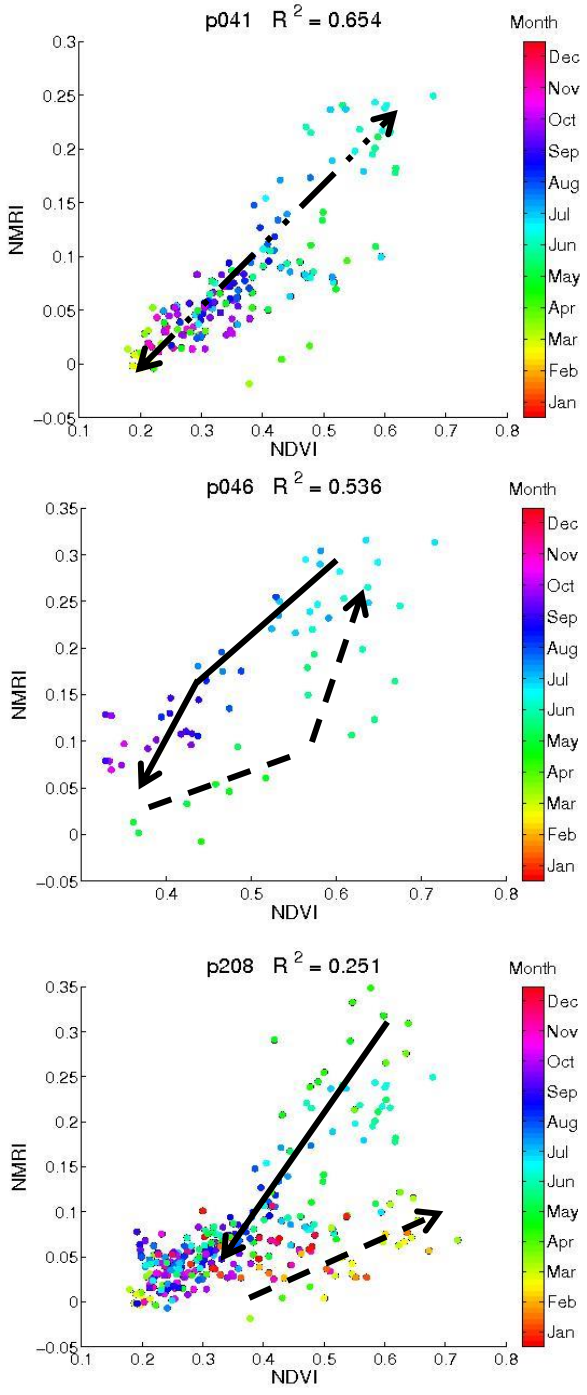

Figure 6. Annual correlation cycles for p041, p046, and p208 (see Fig. 3 for locations). Each point represents one NDVI sample day on which NMRI data has also been extracted for 2007-2012. Dashed lines represent vegetation greenup while solid lines illustrate vegetation decline following senescence.

p046 in Bonner, Montana has a lower correlation than p041 (R^2=0.54) due to cyclical stratification by month (Fig. 6, middle plot). In April and May, NDVI respond strongly while NMRI signals increase only slightly. In early June, NMRI increases and NDVI remains constant. For the remainder of the growing season, NMRI and NDVI decline together. We observe a similar but more extreme pattern at Mediterranean California site p208 (see Figure 2 for time series) in Williams, California (R^2=0.25). Here (Fig. 6, bottom plot) NDVI signals respond sooner than NMRI at the start of the growing season. Then both signals trend linearly together after senescence. Greenup occurs earlier in the season at this site than at the Colorado (p041) and Montana (p046) sites. This site has a lower correlation value due to both the change in slope immediately after late season senescence, and the large amount of time the vegetation is dry and with a stagnant, low signal.

These three sites, each with different cycles, illustrate temporal variation in vegetation growth. They also serve to highlight vegetation complexities that are not conveyable in correlation values. Correlation results, presented below, need to be regarded with this heterogeneity in mind.

3.2.b Correlation by region

Site-by-site average R^2 values range from 0.00 to 0.78 (mean=0.31±0.2, median=0.28) (Table 1). Correlation results are distinct when viewed by regional averages. Those regions that fall in temperature-limited areas such as Montana, northern Utah, Idaho, Colorado, Wyoming, and eastern Oregon (mountains and prairies) exhibit high R^2 values (0.46±0.2 and 0.49±0.1, respectively). Western California sites (Mediterranean California) in precipitation-limited regimes display low R^2 values (0.26±0.2); shrub sites have a lower correlation value than grasslands. The lowest R^2 correlations are in insolation-constrained sites in western Oregon and

Washington (coast: 0.10±0.1). In addition to these end-member populations, desert sites in Nevada and eastern California with noisy, low range signals also have an intermediate R^2 (0.37±0.2). When viewed more closely, Mediterranean California (n=99) sites subdivide into lower R^2 values towards to coast, and high values inland, ranging from 0.00 to 0.67 (mean= 0.25, median=0.23).

3.2.c Lag effects and correlation

Obtaining NMRI points with a specified lag time from NDVI data produces an increase

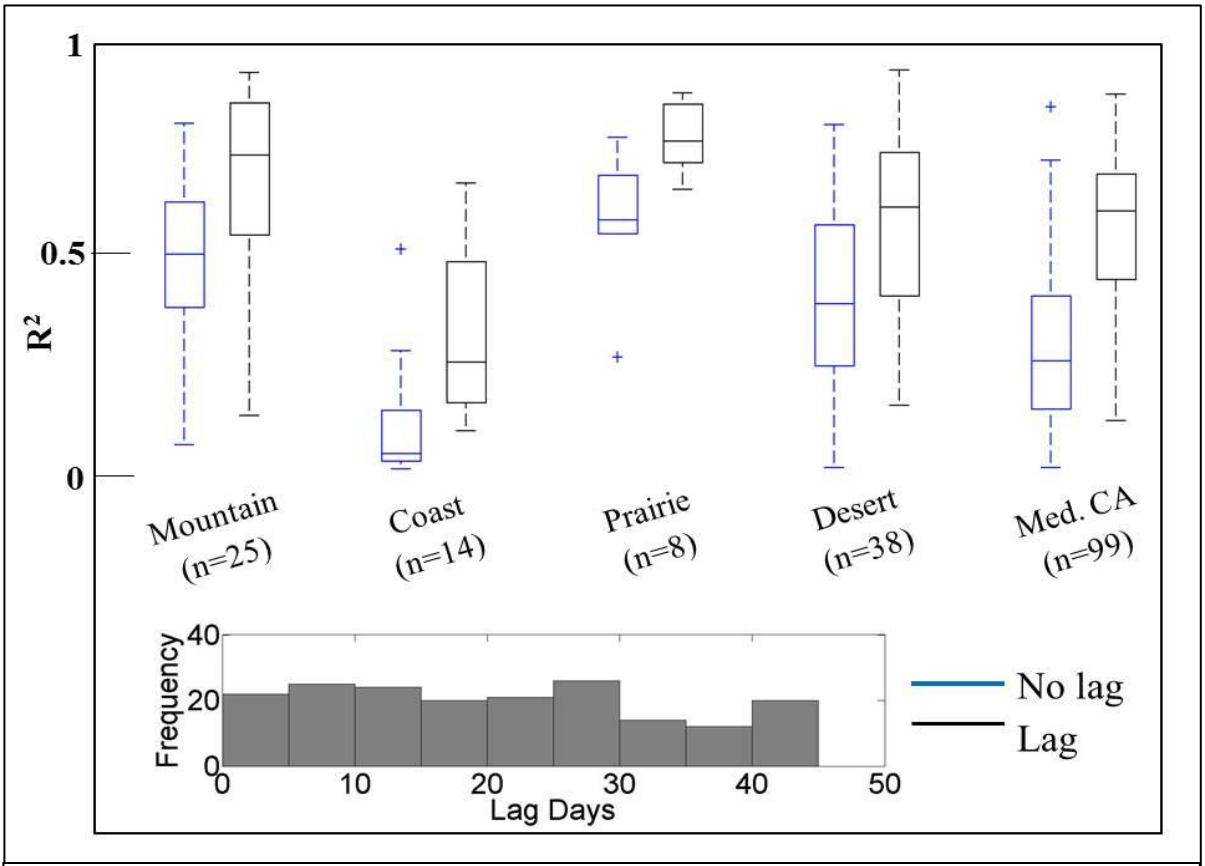

Figure 7. NDVI versus NMRI correlations grouped by land cover type. For each land cover type, correlations without lag are on the left in blue and maximum lagged correlations are on the right in black. Plot displays outliers (+), median, quartiles, maximum, and minimum values. Inset histogram shows correlation results increase with a lag up to 21 days and then decrease. The highest lag days (>40 days) are found at coastal sites both in the coast and Mediterranean California subdivisions.

in correlation (Fig. 7). Correlation increases with lag at many sites; the strongest correlation is at an average lag of 21 days. When including lag effect, maximum R^2 values increase, ranging from 0.08 to 0.86 (mean= 0.53±0.2, median =0.57) (Table 1). The highest and lowest R^2 values remain in the same regions: prairies and coasts (0.72±0.1 and 0.28±0.2, respectively) (Fig. 7). Overall, R^2 values and lag times are inversely correlated (Fig. 8): maximum R^2 values (Fig. 8a, blue points) are highest in the prairies and mountains where lag days are the least (Fig. 8b, yellow points). Minimum R^2 values (Fig. 8a, tan points) are in the coast regions where lag days are the most (Fig. 8b, red points).

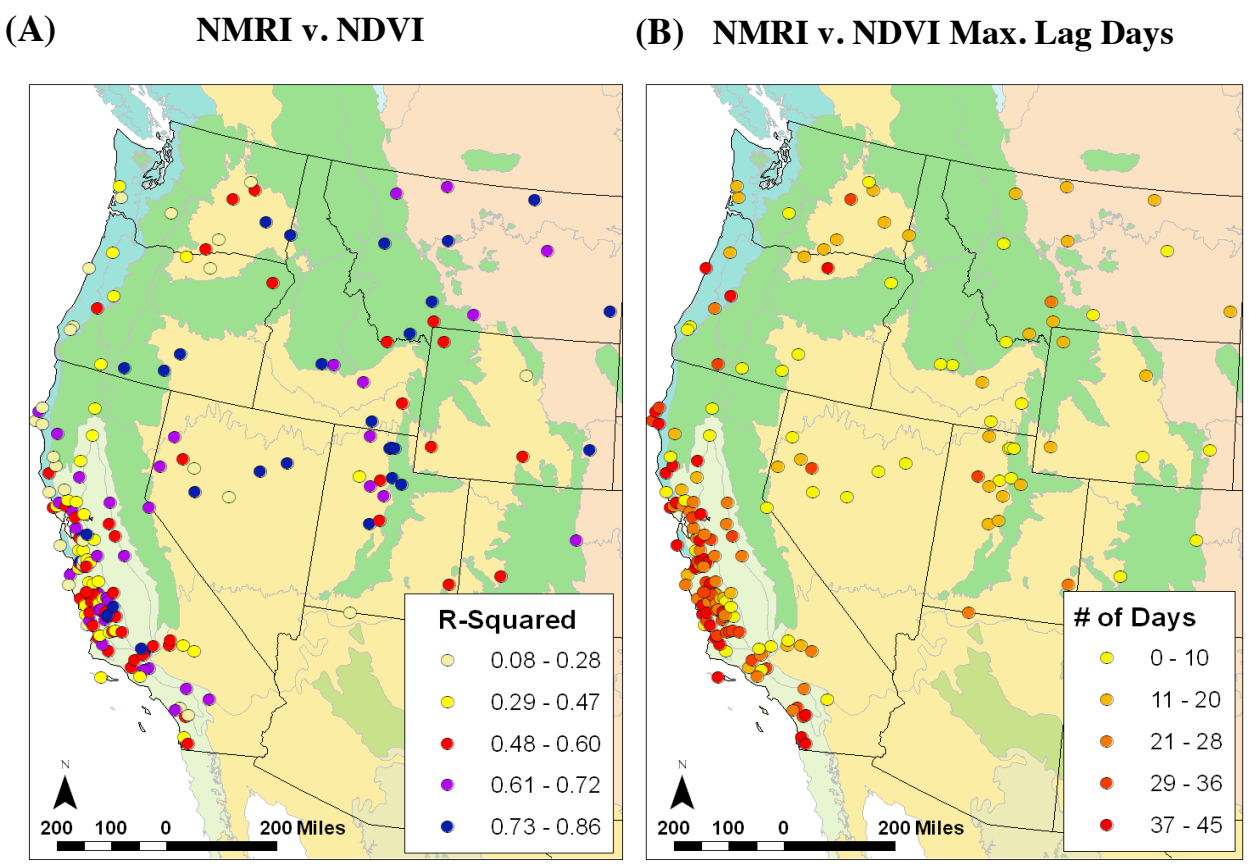

Figure 8. The left panel shows maximum R^2 values ranging from 0.082 to 0.863 with a mean value of 0.527. The right panel displays the number of days required site-by-site to produce the strongest correlation. The coast and Mediterranean California sites (see Table 1) increase in correlation results as lag increases up to 27 days, though many still have relatively low R^2 values. Prairie, desert, and mountain sites require only 9 to 15 days of lag to achieve their maximum R-squared value which has higher correlation than coast sites.

When lag days are clustered by region (Fig. 9) regional trends from Figure 8b become more apparent. On average sites in the mountains region peak at 9 days, coast at 27 days, prairie at 10 days, deserts at 15 days, and sites in Mediterranean California at 27 days. The highest lag days (>40 days) are found at coastal sites both in the coast and Mediterranean California subdivisions. Zero or potentially negative lag days are found in the desert, coast, and mountain sites. Coast sites have the greatest variability between lag days. Mediterranean California sites most closely match the average trend of the whole population seen in Figure 7.

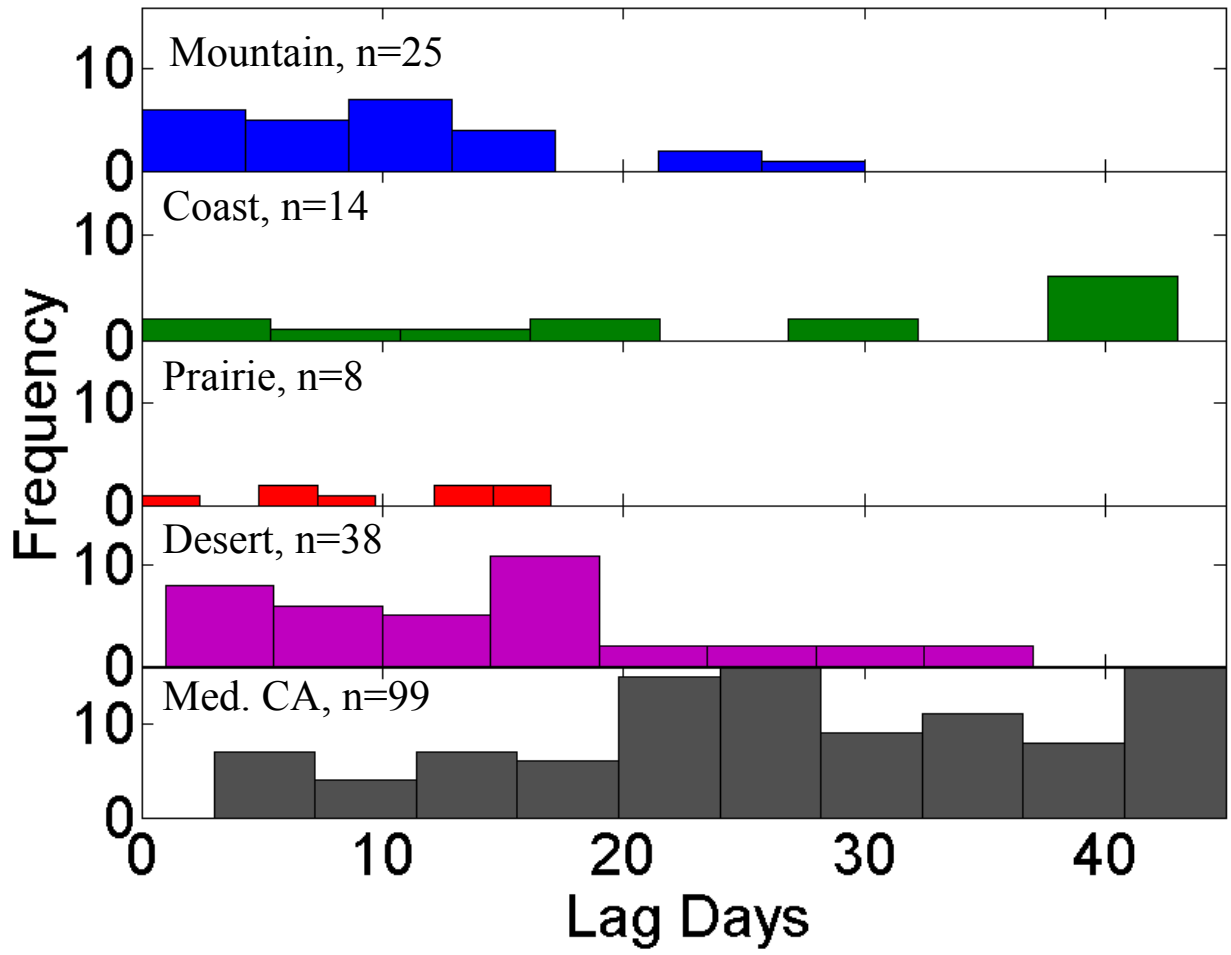

Figure 9. These hisotrgrams display the number of days required by region to produce the strongest correlation. Region names and total population numbers are reported in the upper left hand corner for each plot.

Results are consistent with the conceptual model for vegetation influences on NMRI (Small et al., 2010). Initial greening of leaves and increases in photosynthetic activity yields early, high NDVI results whereas the effect of vegetation growth on NMRI is only apparent after increasing photosynthetic activity produces additional plant growth. The average lag between these two increases is 21 days. This observation is consistent with previous measures that support multipath variations lag NDVI by approximately three weeks (Small et al., 2010).

3.3 Relationship between NMRI and NDVI phenology metrics

3.3.a Phenology metrics: Five water-year time series (2008-2012)

Phenology metric results are presented in Table 2 and Figure 10. NMRI and NDVI SOS dates are slightly correlated for the five water-year record (R^2=0.16, p=0, n=865). On average increases in NDVI precede that of NMRI by 52 days. NDVI SOS has an average doy of 18

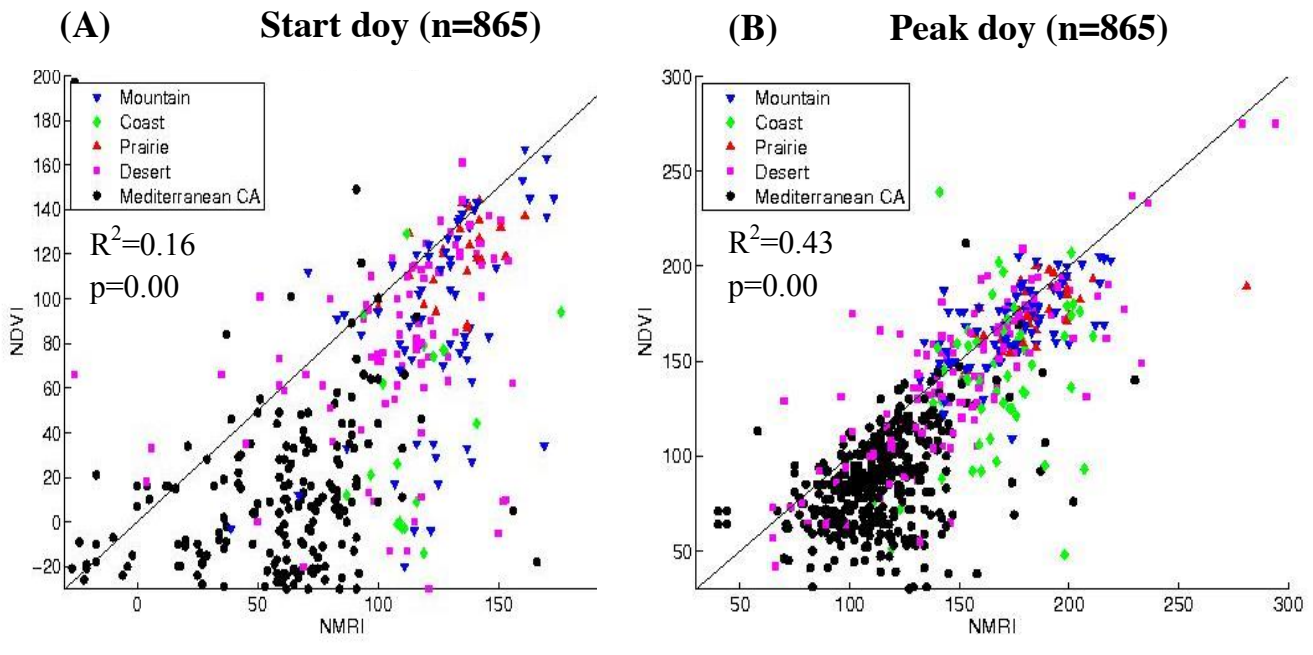

Figure 10. SOS doy and peak vegetation doy NDVI versus NMRI colored by regions. Each point represents one water-year of data for one site (173 sites for 5 water-years yields 865 points).

while NMRI SOS has an average doy of 70 (Table 2). Low correlation suggests the data are a mix of regionally grouped populations.

Grouped by region, SOS is earliest for Mediterranean California sites (Fig. 10a, black circles), followed by coast (green diamonds), desert (purple square), mountain (blue triangle), and finally prairie sites (Fig. 10a, red triangle). Results differ depending on the metrics used: NMRI places SOS for mountain sites 25 days later than NDVI (Table 2). Coast sites differ by

2008-2012	**SOS (doy)**	**Season Length (days)**	**Peak Doy**
NDVI Avg.	18	171	110
NMRI Avg.	70	133	137
Mountain (n=22)			
NDVI	87	138	169
NMRI	112	118	176
Coast (n=14)			
NDVI	4	233	135
NMRI	106	130	167
Prairie (n=8)			
NDVI	110	124	176
NMRI	130	105	189
Desert (n=30)			
NDVI	60	140	142
NMRI	107	119	161
Mediterranean California (n=99)			
NDVI	-16	179	83
NMRI	42	136	111
Grasslands (n=66)			
NDVI	-13	177	83
NMRI	47	128	113
Shrubs (n=33)			
NDVI	-20	182	82
NMRI	32	150	107

Table 2. Phenology metrics extracted for NDVI and NMRI. Overall NMRI has a later SOS, later peak doy, and shorter season length. Mediterranean California sites are subdivided into grasslands and shrubs.

102 days, prairie sites by 21 days, and desert and Mediterranean California sites by 26 days each (Table 2). Figure 11 illustrates these results spatially. Sites farther north and west have a later SOS doy (Fig.11a, blue points) while sites in California have an earlier SOS doy (Fig.11a, red points). The difference between SOS extracted by NDVI and NMRI, respectively, is greater in western sites (Fig. 11b, red points) than eastern ones (Fig.11b, blue points).

Season length has lower correlation between indices (R^2=0.08, p=0, n=865) than SOS. When found by NMRI, average season length is 133 days compared to 171 days by NDVI (Table 2). Season length is longer at all regional sites when recorded by NDVI instead of NMRI. The maximum difference in season length by region is 103 days at coast sites. The minimum difference is 19 days at desert sites (Table 2). Season length is not plotted, as results duplicate those of SOS.

NMRI and NDVI peak vegetation growth dates exhibit the highest correlation for the five water-year record (R^2=0.43, p=0, n=865). On average, NMRI finds that vegetation peaks on doy 137 and NDVI on doy 110 (Table 2). By region, sites in Mediterranean California peak earlier than other sites (Fig. 10b, black diamonds). NMRI and NDVI place mountain and prairie sites vegetation peaks on relative equal days (Fig.10b, blue triangle and red triangle are on 1:1 line). Peak doy for these two regions is later than other sites (Fig. 11c, blue points). NMRI determines that coast and desert sites vegetation peak later than NDVI (by 32 and 19 days, respectively). These sites still cluster around the 1:1 line (Fig. 10b, green diamond and purple square), and are spread, especially in desert sites, from the maximum to minimum peak doy (Fig. 10b, purple square). Figure 11c illustrates distinct peak doy clusters by region. Sites to the north peak later (Fig. 11c, blue points) while sites throughout California peak earlier (Fig. 11c, green points). The earliest peak doy is in the Central Valley (Fig. 11c, yellow and red points). Overall,

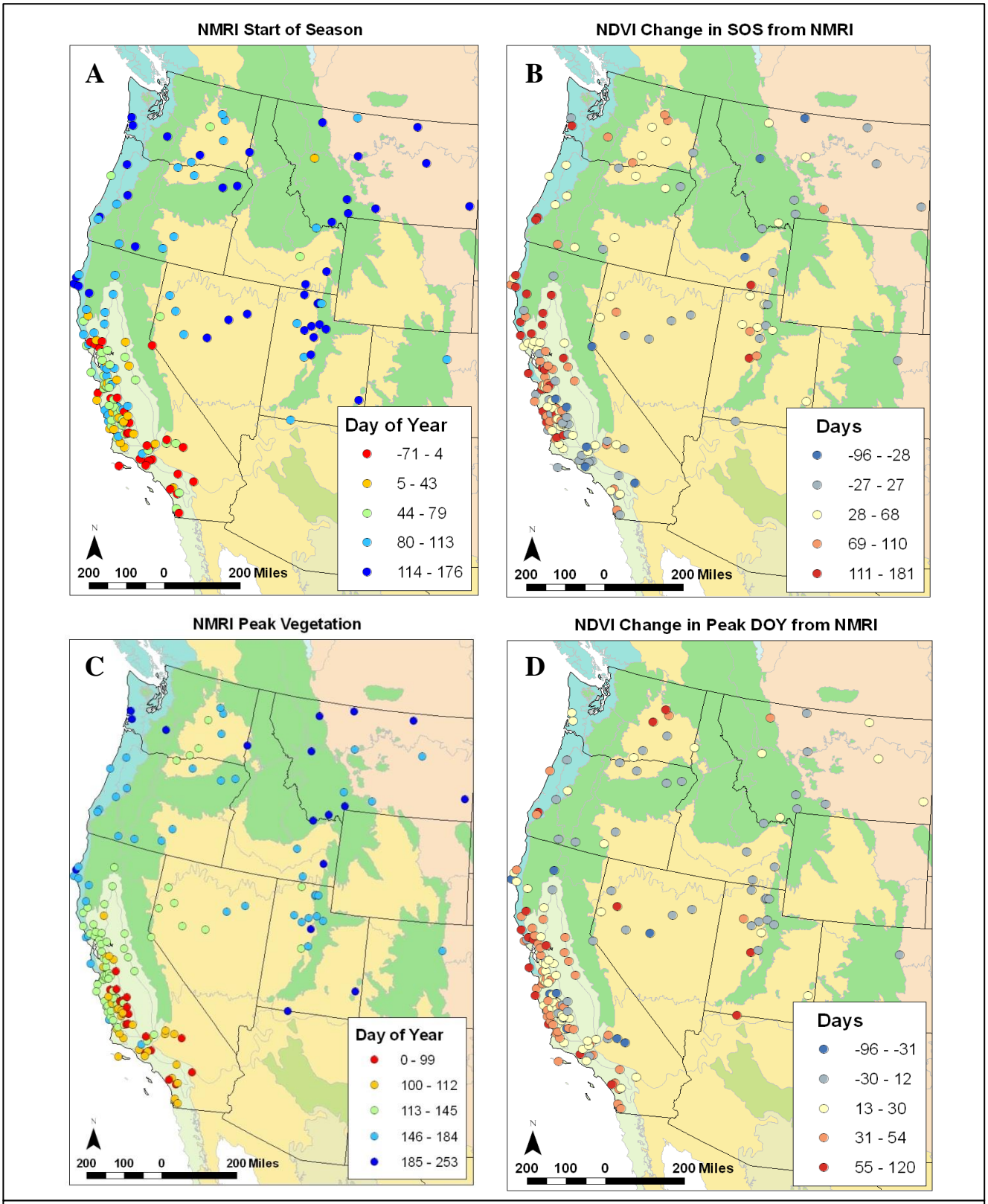

Figure 11. Phenology metrics extracted for NDVI and NMRI: (a) Start of season (SOS) doy from NMRI; (b) change in SOS doy (NMRI-NDVI), positive numbers have a later NMRI SOS doy than NDVI; (c) peak vegetation doy extracted from NMRI; (d) change in peak doy (NMRI-NDVI).

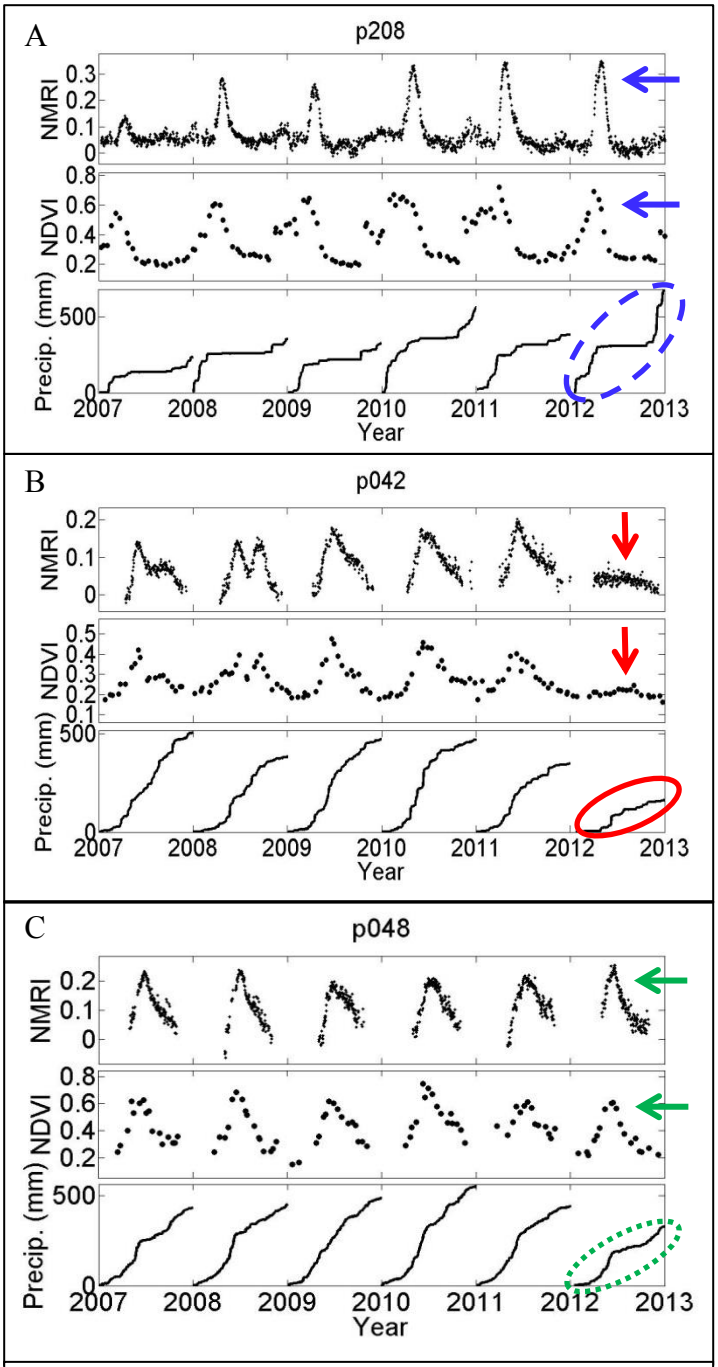

Figure 12. NMRI and NDVI record for sites (a) p208, (b) p042, (c) p048. Note the 2012 above average precipitation at p208 (dashed blue circle) and below average precipitation at p042 (solid red circle) and the effect on NMRI and NDVI signals. P048 has below average precipitation (dotted green circle) but this does not affect NDVI and NMRI metrics.

phenology metrics extracted by microwave NMRI record a later start of season, later peak day of year, and shorter season length than determined by optical NDVI.

3.3.b 2012 drought variability

High temperature and low precipitation patterns in the spring and summer of 2012 not only set many climatic records across the United States, but created a drought which affected a historically large fraction of the country (Karl et al., 2012). In Figure 12 sites p208, p042, and p048 highlight the variability of drought extent. Both p208 and p042 were classified as having a "severe drought" in 2012 while p048 was only "abnormally dry" (National Drought Mitigation Center; http://droughtmonitor.unl.edu/). Site p208 in Williams, California (see Fig.3 for location) had 669 mm of precipitation in 2012 (Fig. 12a, blue circle), an increase of 249 mm from average (2008-2012). With an increase in precipitation in 2012, NMRI

and NDVI responses are constant from previous years (Fig. 12a, blue arrows). Site p042 in Wheatland, Wyoming (see Fig. 3 for location) had 162 mm of precipitation in 2012, a decrease of 228 mm from average (Fig. 12b, red circle). This decrease in precipitation caused a drastic decrease in NMRI and NDVI responses (Fig. 12b, red arrows). Site p048 in Bozeman, Montana (see Fig. 3 for location) had 328 mm of precipitation in 2012, a decrease of 122 mm from average (Fig. 12c, green circle). Here, decreased precipitation did not influence the 2012 NMRI and NDVI signals (Fig. 12c, green arrows). It may, however, have an effect on 2013 data. Due to variability in drought influence, as suggested by these sample sites, results below need to be regarded as an approximation.

3.3.c 2012 drought results

The effect of the 2012 drought averaged over all stations (n=173) strongly influences metric amplitude but not phenology indexes. In 2012 NMRI and NDVI SOS and peak doy did not deviate far from average values. Season length was shorter in 2012 due to an earlier end of season.

2008-2012	**SOS (doy)**	**Season Length (days)**	**Peak Doy**	**Amplitude**
NDVI Avg.	18	171	110	0.265
NMRI Avg.	70	133	137	0.133
2012	**SOS (doy)**	**Season Length (days)**	**Peak Doy**	**Amplitude**
NDVI Avg.	21	148	112	0.203
NMRI Avg.	66	123	141	0.117

Table 3. Seasonality parameters for 2012 verse 2008-2012 averages. Season length was shorter in 2012 and peak vegetation doy was slightly later. 2012 amplitude values were lower compared to average.

In 2012 NMRI and NDVI SOS dates (Table 3) are slightly later than average (NDVI: doy 21 (2012) v. 18 (average); NMRI: doy 66 v. 70). NDVI SOS dates are earlier than NMRI, consistent with data from the five water-year time series. Peak doy was later overall in 2012

than average (NDVI: doy 112 v. 110; NMRI: doy 141 v. 137). This relationship was more prevalent in the NMRI than the NDVI data, though not significantly. Season length in 2012 was less than average, although the deviation was larger for NDVI (NDVI: 148 v. 171 days; NMRI: 123 v. 133 days).

Seasonality amplitude varies more than phenology indexes with drought. Whereas in Section 3.1 reported range amounts represent the difference between maximum and minimum values throughout the entire data set, those obtained in Table 3 are from the maximum and minimum values of the seasonality data and only extend through the SOS doy and EOS doy for each year. This causes smaller values than values reported previously (Table 1). Both NMRI and NDVI minimum amplitude values are presented for 2012 (Table 3). Data in 2012 deviated by 33% from the mean (2008-2012) for NDVI and 22% for NMRI.

3.4 NMRI and NDVI seasonality metrics as a function of climatic variables

The effects of climate variables on NMRI and NDVI SOS and peak doy are presented in Figure 13. Statistics are presented in Table 4. Mean annual temperature will be discussed, followed by mean annual precipitation, and finally, latitude.

3.4.a Mean Annual Temperature

Mean annual temperature (MAT, ºC) plays a moderate role (R^2=0.26, p=0, n=865) in correlation with SOS doy from NMRI metric (Fig. 13g). As MAT decreases, NMRI SOS increases. Correlation values between MAT and NDVI are slightly higher (R^2=0.30, p=0, n=865) and exhibit negative relationship; as MAT decreases, SOS doy increases (Fig. 13e). Stratification is evident around 4ºC (Fig. 13e).

MAT has the most significant relationship to peak doy (R^2=0.59, p=0, n=865) for the NMRI metric (Fig. 13h) and the NDVI metric (R^2=0.45, p=0, n=865) (Fig. 13 f). Both have a linear, negative relationship: as MAT decreases peak doy increases, with NMRI doy occurring slightly after NDVI peak doy. Season length does not have significant correlation with MAT and is not shown in Figure 13 (Table 4).

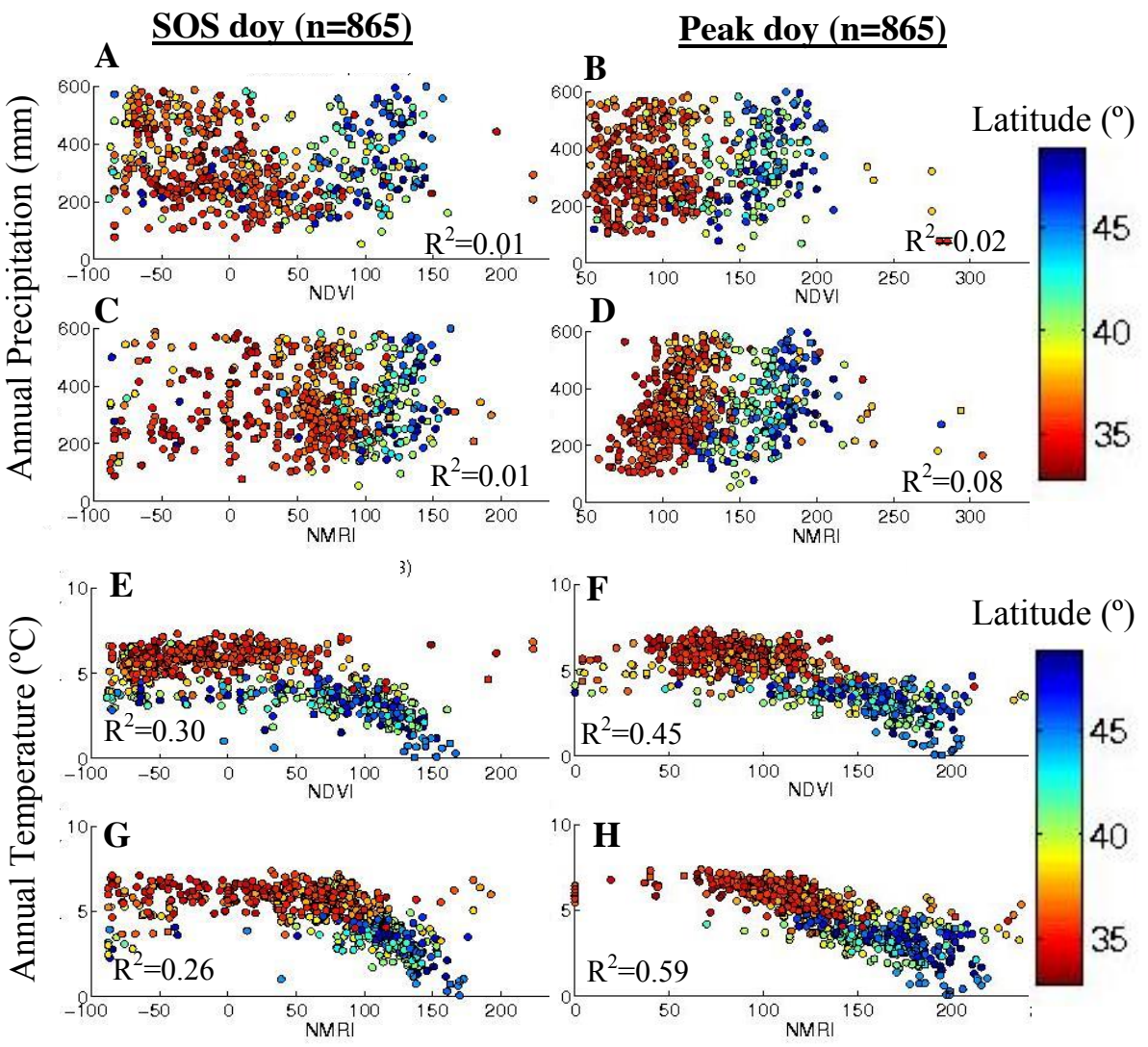

Figure 13. Start doy (a,c,e,g) and peak vegetation doy (b,d,f,h) organized by mean annual precipitation (a-d) and mean annual temperature (e-h) and NMRI (c,d,g,h) or NDVI (a,b,e,f) and stratified by latitude. Each point (n=865) represents one water-year of data for one site (2008-2012).

3.4.b Mean Annual Precipitation

Mean Annual Precipitation (MAP, mm) does not exert a significant influence on phenology metrics. With an increase in MAP, SOS doy generally increases (Fig. 13a and c). This relationship corresponds equally to NMRI and NDVI indexing (NMRI R^2=0.01, p=0.05; NDVI R^2=0.01, p=0.04, n=865). Season length also exhibits a positive linear relationship, but with stronger NDVI correlation (NMRI R^2=0.09, p=0; NDVI R^2=0.29, p=0, n=865). This is in stark contrast to the low correlation of season length with MAT (Table 4). MAP correlates linearly with peak doy (Fig. 13b and d), as sites with greater MAP have a later peak doy (NMRI R^2=0.08 p=0; NDVI R^2=0.02 p=0, n=865). As evidence by reported correlation values, there is not significant correlation between peak doy and MAP.

Climate Variable	Phenology Metric	Index	R^2	p-value
Mean Annual Temperature	SOS	NMRI	0.26	0.00
		NDVI	0.30	0.00
	Season Length	NMRI	0.00	0.23
		NDVI	0.00	0.21
	Peak doy	NMRI	0.59	0.00
		NDVI	0.45	0.00
Mean Annual Precipitation	SOS	NMRI	0.01	0.05
		NDVI	0.01	0.04
	Season Length	NMRI	0.09	0.00
		NDVI	0.29	0.00
	Peak doy	NMRI	0.08	0.00
		NDVI	0.02	0.00

Table 4. Phenology correlation and p-values, $p \leq 0.05$ for R^2 to be significant (n=865).

3.4.c Latitude

With direct correlation to MAT and MAP, latitude influences NMRI and NDVI extracted phenology indexes (Fig. 13). With an increase in latitude, NMRI and NDVI determined SOS

doy increases (Fig. 13a,c,e, and g; cool colors increase to the right). For SOS metrics (Fig. 13a and c) MAP has a stratified, direct correlation with latitude while MAT does not (Fig. 13e and g). Season length does not correlate with latitude for NMRI or NDVI, though it stratifies by MAT. As latitude increases, vegetation peak doy increases for both NMRI and NDVI (Fig. 13b,d,f,h). NMRI predicts relative later peak doy than NDVI (Fig. 13d points are clustered further to the right than Fig.13b). MAT separates sites along peak doy where low latitude sites have higher MAT than high latitude sites (Fig. 13f and h). MAP does not stratify by latitude for peak doy (Fig. 13b and d).

CHAPTER 4

Discussion

NMRI and NDVI correlation, lag, and phenology are spatially variable. Correlation between NMRI and NDVI is lowest in the coast region and highest inland in mountain and prairie regions. NMRI variations lag NDVI by approximately 21 days, causing an increase in correlation for all regions. When determined by NMRI versus NDVI, phenology metrics are offset spatially with the largest offsets along Pacific Ocean coastline, decreasing inland and subdivided by region. Thus we see that coast regions have the low correlation, longest lag days, and biggest offset of phenology metrics. Mountain and prairie sites represent the opposite end member. Mediterranean California and desert sites have intermediate results.

These results will be expanded and discussed in the conceptual lens of regional climate influences on vegetation. First, we will present temperature-limited sites including the regions of mountain, prairie, and desert, followed by precipitation-limited regions of Mediterranean California and deserts, and finally, a discussion of insolation-limited costal sites. We will conclude with remarks on the 2012 drought.

4.1 NMRI constrains and bias

4.1.a Temperature-limited regions

Temperature-limited regions such as Montana, eastern Washington, eastern Oregon, and Idaho (subdivisions of mountain, prairie, and some desert) are characterized as having a MAT of 1°C to 10°C with MAP of 700-3,000 mm (Wiken et al., 2011). From our analysis, these sites have intermediate NMRI and NDVI range values. They have the highest R^2 correlation values with NDVI, and improve in correlation with increase in data lags of 9 to 15 days. At example

site p046 there is a well correlated, cyclical greenup and post-senescence cycle (Fig. 6). Phenological metrics from these sites have a slightly later SOS doy and peak doy determined by NMRI than NDVI, and a longer season length recorded by NDVI than NMRI. This deviation is less evident than for other regions. Compared to other regions, the SOS doy and peak doy is later and season length is shorter. There is an inverse relationship between MAT and SOS doy and peak doy.

In temperature-limited areas, winter temperatures prevent vegetation growth until there is an increase in soil and air temperatures (Nemani et al., 2003). After thawing, transpiration rates drive water into existing branches and leaves causing an increase in vegetation water content prior to new green leaf construction (Jones et al., 2012). This suggests that there should be an increase in vegetation water content before greenness. However, our phenology results support that in these temperature-limited regions plants generally grow and green concurrently. Thus we see a response in microwave NMRI that echoes the timing of that of optical NDVI. These responses to greening and growing occur later in the season than in regions constrained by insolation or precipitation. This, however, may be attributed to our selection of grassy sites, and exclusion of shrubs sites and those with >50% woody vegetation cover.

4.1.b Precipitation-limited regions

Water constrained regions such as those in Mediterranean California have a high MAT of 14°C to 18°C and MAP of 200-1,400 mm, though many GPS sites are located within the lower end of this precipitation range (Wiken et al., 2011). Results suggest that these sites have high NMRI and intermediate NDVI range values, and relatively low R^2 values, with correlation decreasing towards the coast. Site p208, an example of a water-limited site, exhibits relatively low correlation due to its rapid greenup period where NDVI and NMRI indexes do not correlate

(Fig. 6). Correlation increases at these sites with an increase of lag time by as much as 28 days. Mediterranean California sites have a later SOS doy for NMRI than NDVI records. These sites also have a later peak doy when determined by NMRI. Season length is shorter for NMRI than NDVI. Compared to other regions, SOS and peak doy is earlier and season length is longer. MAP exhibits a positive linear relationship with SOS doy and has higher correlation in this region than others.

In seasonally-arid ecosystems, activation of photosynthetic material and resultant greening occurs rapidly after initial precipitation events (Huxman et al., 2004). This results in concurrent greenup and vegetation water content responses. However, areas dominated by croplands have a delay in greenup followed by an increase in water content (Jones et al., 2012). In these agricultural settings, greenup occurs at seed germination often before biomass accumulation; increases in vegetation water content are delayed until the plant puts on above-ground biomass (Wigneron et al., 1997). After initial plant growth, plants senescence quickly, and thus have a relatively short season length. Similarly, there is a delay in water content responses in areas with high woody vegetation cover (Jones et al., 2012). Many of our Mediterranean California sites are croplands or contain natural woody vegetation including chaparral and oak woodlands and should therefore, echo these observations (Wiken et al., 2011). Indeed, the delayed, quick response of NMRI to phenology metrics and lack of correlation between NDVI and NMRI matches these observations: greenup occurs before increases in vegetation water content.

An analysis of water-limited populations would be incomplete without mention of desert sites in the central Great Basin. This region occupies a large portion of Nevada and western Utah, with small extensions into California and southern Idaho. These sites have a MAT of 2°C

on high mountains to 14°C in southern lowland and MAP of 4-1,000 mm (Wiken et al., 2011). Sites here have low NMRI range and especially low NDVI range signals. They have a relatively low to medium R^2 correlation (0.32 to 0.42) that improves with a 15 day lag. Many of these sites have low annual vegetation growth and greening, creating noisy, low amplitude NDVI data and sporadic NMRI data. This makes it difficult to extract phenology parameters and correlation values. Some sites in this region may have an inexact NMRI normalization; we see higher amplitude variation than we would predict for NMRI, thus the normalization is overemphasizing the NMRI signal. These sites should not necessarily be clustered with other water-limited population without first evaluating total amount of vegetation biomass and NMRI normalization.

4.1.c Insolation-limited regions

Though not a very spatially homogenous, sites in western Washington and Oregon (coast) with alpine to temperate rainforests, highlight the influence of insolation-limitations on NMRI and phenology metrics. Sites have MAT of 7°C to 14°C and MAP of 900-5,000 mm (Wiken et al., 2011). Vegetation at these sites is dominated by woody cover with oak savanna and oak woodlands (Wiken et al., 2011). These sites have the lowest NMRI range values, but the second highest NDVI range values, generating the lowest R^2 correlation values (Fig. 4a and b). Similar to water-constrained locations, correlation at these sites increases with an increase of lag time by as much as 26 days. Sites have a later SOS and peak doy for NMRI than NDVI records. Season length is almost half as long when found by NMRI. Due to large differences between NMRI and NDVI determined phenology, compared to other regions, event timing ranges from early (by NDVI) to late (by NMRI). Season length determined by NDVI is longer than for any other region.

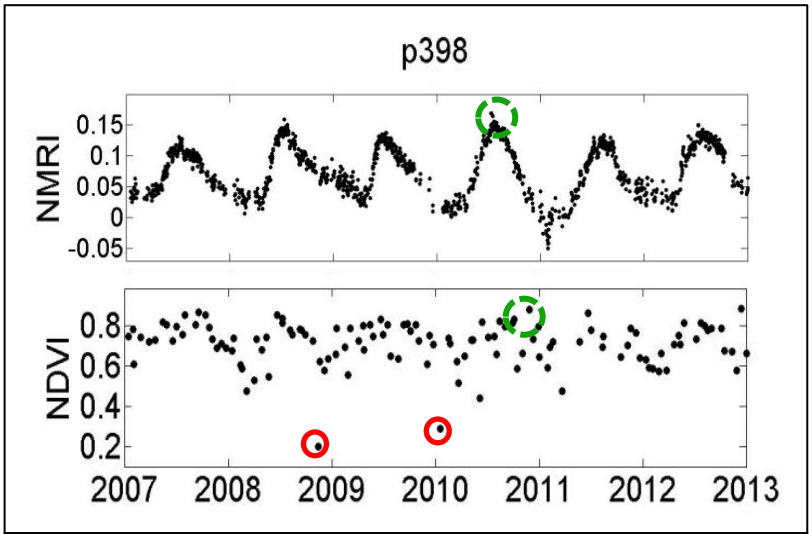

Figure 14. Clean NMRI and NDVI signal for site p398. Note the outlier NDVI points around 0.2 (solid red circles) and the NDVI versus NMRI late season peak in 2010 (dashed green circles).

NMRI records at these sites with woody vegetation cover are similar to those in Mediterranean California; they highlight the delay between greenup and addition of water content. However uniquely from those in California, these sites also emphasis the shortcomings of NDVI in insolation-limited, cloud covered regions. Site p398 in Aberdeen, Washington located approximately six miles from the Pacific Ocean (see Fig. 3 for location) has a clean NMRI signal but very noisy NDVI signal (Fig. 14). A noisy NDVI signal at insolation-limited sites like p398 is likely due to the fact that NDVI has a different footprint size than NMRI and is influenced by forests or other land cover types. The high average NDVI value (~0.7) at site p398 (Fig. 14) likely reflects the presence of forested areas.

4.2 Drought

The 2012 drought recorded early spring warmth that led to early greenup (SOS) followed by rapid deterioration of vegetation greenness across much of the United States (Karl et al., 2012). Our phenology analysis for 2012 versus 2008-2012 averages does not show any clear relationships in an early SOS or peak doy. It does, however, trend towards a shorter season length in 2012.

While the 2012 drought did affect a historically large fraction of the country, only 39% of the country was classified as being in severe to extreme drought. This is in stark contrasts to the 1930s when as much as 63% of the country was experiencing extreme drought (Karl et al., 2012). Early on, the 2012 drought affected mostly Texas and the southern United States (Fig. 15a). Some of California was influenced, but not where the majority of our GPS sites are located. No sites in Montana, Wyoming, Utah, or Colorado were considered under "moderate drought". By July 3rd, a greater percent of the country was under drought conditions, including more locations with GPS stations (Fig. 15b).

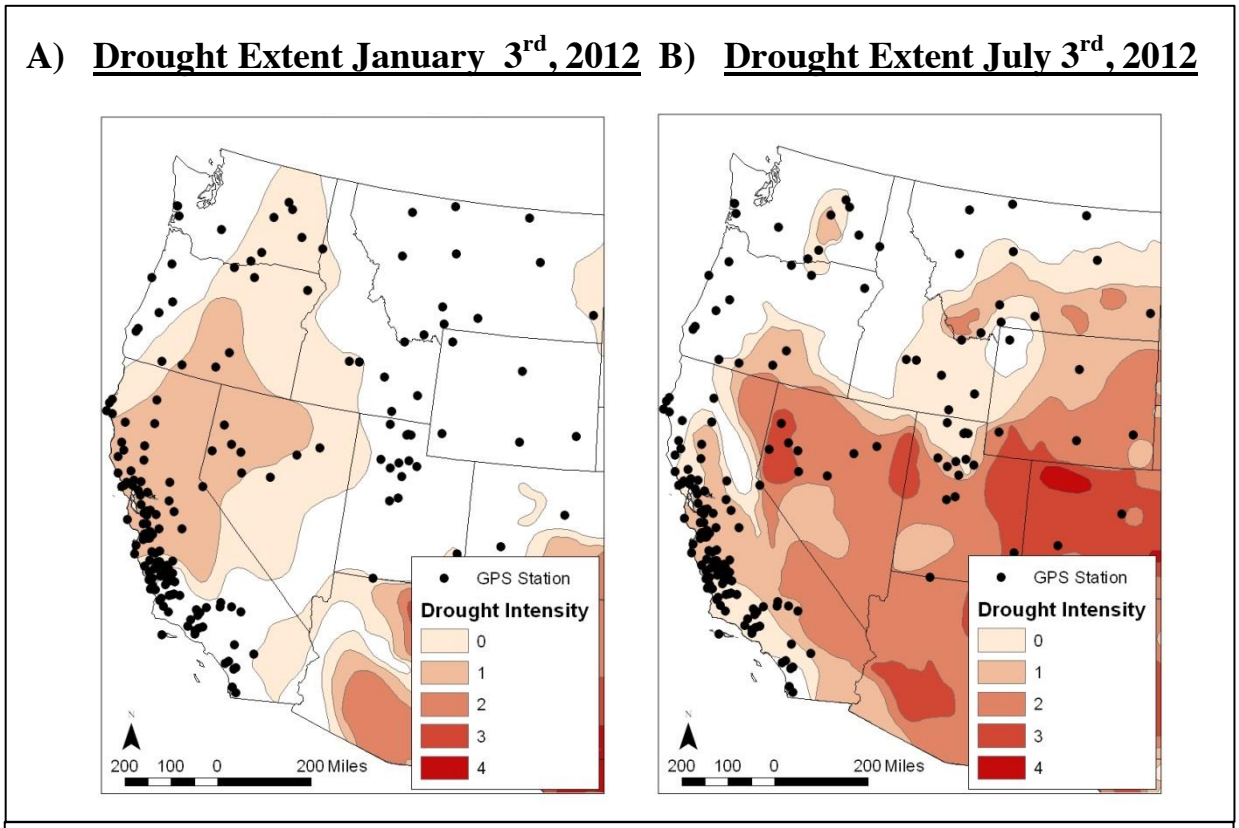

Figure 15. Extent of 2012 drought on January 3rd (left) and July 3rd (right). Note how few GPS sites are in a drought intensity of two or higher. Intensity of zero is abnormally dry, one is drought-moderate, two is drought-severe, three is drought-extreme, and four is drought-exceptional (National Drought Mitigation Center at the University of Nebraska-Lincoln).

The increase in late season drought extent caused quick deterioration of vegetation, making end of season dates earlier than previous years. This resulted in a shorter season length for vegetation at GPS sites. Thus, as observable in our NMRI and NDVI data, we see that the drought in 2012 had a limited effect on SOS but did influence the end of season, which is recorded by a shortening of season length. This is supported by our amplitude data that deviated from the mean in 2012 by 33% for NDVI and 22% for NMRI.

CHAPTER 5

Conclusions

The scattering index NMRI provides a daily monitoring tool that has shown great potential as a continuous, all-weather, and close to real-time microwave radar system for monitoring vegetation state. NMRI is sensitive to plant growth in vegetation types that together cover a majority of the Earth's land surface, including croplands, grasslands, and shrublands. Phenology metrics extracted from NMRI data are sensitive to biomass changes that are independent of, yet linked with, plant chlorophyll content from satellite optical remote sensing NDVI.

Overall, NMRI has improved retrievals over NDVI and is particularly better for retrieving clean signals at insolation-limited coastal sites. NMRI and NDVI correlation is a function of location where NMRI variations lag NDVI by approximately 21 days; consistent with the idea that greenup precedes plant growth. In terms of phenology metrics, NMRI extracted SOS is later, peak doy is later, and season length is shorter than when determined by optical NDVI. This suggests that greenup lasts for longer than plant growth. Phenology metrics are offset spatially with the largest offsets along Pacific Ocean coastline, decreasing inland and subdivided by region, supporting that plant growth cycles are controlled by regional climates. Drought has a variable influence on regional vegetation and needs further understanding before drought years can be accurately recorded by NMRI and NDVI indexes.

These results, along with previous GPS-IR analyses and success from other satellite microwave detection system indicate a strong prospect for satellite microwave remote monitoring of vegetation. GPS-IR systems should be further evaluated, particularly in the Midwest and eastern United States for accuracy.

Bibliography

Al-Bakri, J., and Taylor, J., 2003, Application of NOAA AVHRR for monitoring vegetation conditions and biomass in Jordan: Journal of Arid Environments, v. 54, no. 3, p. 579–593, doi: 10.1006/jare.2002.1081.

De Beurs, K.M., 2008, Lecture 2: Modeling of Land Surface Phenology with satellite imagery, *in* Madison LSP Workshop.

Box, E.O., Holben, B.N., and Kalb, V., 1989, Accuracy of the AVHRR vegetation index as a predictor of biomass, primary productivity and net CO2 flux: Vegetatio, v. 80, no. 2, p. 71–89, doi: 10.1007/BF00048034.

Brakke, T., Kanemasu, E., and Steiner, J., 1981, Microwave radar response to canopy moisture, leaf-area index, and dry weight of wheat, corn, and sorghum: Remote Sensing of Environment, v. 220, p. 207–220.

Burke, I.C., Kittel, T.G.F., Lauenroth, W.K., Snook, P., Yonker, C.M., and Parton, W.J., 1991, Regional Analysis of Great the Central Plains Sensitivity to climate variability: Bioscience, v. 41, no. 10, p. 685–692.

Champion, I., and Guyot, G., 1993, Estimating Surface Soil Moisture and Leaf Area Index of a Wheat Canopy Using a Dual-Frequency (C and X Bands) Scatterometer: Remote Sensing of Environment, v. 339, no. March, p. 331–339.

Chen, D., Huang, J., and Jackson, T.J., 2005, Vegetation water content estimation for corn and soybeans using spectral indices derived from MODIS near- and short-wave infrared bands: Remote Sensing of Environment, v. 98, no. 2-3, p. 225–236, doi: 10.1016/j.rse.2005.07.008.

Cihlar, J., St-Laurent, L., and Dyer, J., 1991, Relation between the normalized difference vegetation index and ecological variables: Remote Sensing of Environment, v. 298, no. June 1990, p. 279–298.

Cleland, E.E., Chuine, I., Menzel, A., Mooney, H. a, and Schwartz, M.D., 2007, Shifting plant phenology in response to global change.: Trends in ecology & evolution, v. 22, no. 7, p. 357–65, doi: 10.1016/j.tree.2007.04.003.

Eidenshink, J., 1992, The 1990 conterminous US AVHRR data set: Photogrammetric Engineering and Remote Sensing, v. 58, no. March 1990.

Enquist, C. A. F., Rosemartin, A., and Schwartz, M.D., 2012, Identifying and prioritizing phenological data products and tools: Eos, Transactions American Geophysical Union, v. 93, no. 37, p. 356, doi: 10.1029/2012EO370007.

Estey, L.H., and Meertens, C.M., 1999, TEQC: The Multi-Purpose Toolkit for GPS/GLONASS Data: GPS Solutions, v. 3, no. 1, p. 42–49, doi: 10.1007/PL00012778.

Fischer, A., 1994, A Model for the Seasonal Variations of Vegetation Indices in Coarse Resolution Data and Its Inversion to Extract Crop Parameters: Remote Sensing of Environment, v. 230, no. October 1991, p. 220–230.

Gamon, J.A., Field, C.B., Goulden, M.L., Griffin, K.L., Hartley, E., Joel, G., Peñuelas, J., and Valentini, R., 2012, Relationship Between NDVI, Canopy Structure, and Photosynthesis in Three Californian Vegetation Types: Ecological Applications, v. 5, no. 1, p. 28–41.

Gao, B., 1996, NDWI A Normalized Difference Water Index for Remote Sensing of Vegetation Liquid Water From Space: v. 266, no. April 1995, p. 257–266.

Goetz, S.J., 1997, M ulti-sensor analysis of NDVI , surface temperature and biophysical: International Journal of Remote Sensing, v. 18, no. 1, p. 71–94.

Hargrove, W.W., and Hoffman, F.M., 1999, Using Multivariate Clustering to Charactreize Ecoregion Border: Computing in Sceince and Engineering,, p. 18–25.

Hawkes, R., and Finn, A., 2000, The Effects of Australian Vegetation on GPS, *in* Proceedings of the IAIN World Congress in association with the U.S. ION ANNUAL MEETING, p. 741–754.

Hobbs, R., Yates, S., and Mooney, H., 2007, Long-term data reveal complex dynamics in grassland in relation to climate and disturbance: Ecological Monographs, v. 77, no. 4, p. 545–568.

Holm, A., 2003, The use of time-integrated NOAA NDVI data and rainfall to assess landscape degradation in the arid shrubland of Western Australia: Remote Sensing of Environment, v. 85, no. 2, p. 145–158, doi: 10.1016/S0034-4257(02)00199-2.

Huete, A., 1988, A soil-adjusted vegetation index (SAVI): Remote Sensing of Environment, v. 309, p. 295–309.

Huxman, T.E., Snyder, K., Tissue, D., Leffler, J., Ogle, K., Pockman, W.T., Sandquist, D.R., Potts, D.L., and Schwinning, S., 2004, Precipitation pulses and carbon fluxes in semiarid and arid ecosystems.: Oecologia, v. 141, no. 2, p. 254–68, doi: 10.1007/s00442-004-1682-4.

Jin, S., Feng, G.P., and Gleason, S., 2011, Remote sensing using GNSS signals: Current status and future directions: Advances in Space Research, v. 47, no. 10, p. 1645–1653, doi: 10.1016/j.asr.2011.01.036.

Jin, S., and Komjathy, A., 2010, GNSS reflectometry and remote sensing: New objectives and results: Advances in Space Research, v. 46, no. 2, p. 111–117, doi: 10.1016/j.asr.2010.01.014.

Jones, M.O., Jones, L.A., Kimball, J.S., and McDonald, K.C., 2011, Satellite passive microwave remote sensing for monitoring global land surface phenology: Remote Sensing of Environment, v. 115, no. 4, p. 1102–1114, doi: 10.1016/j.rse.2010.12.015.

Jones, M.O., Kimball, J.S., Jones, L. A., and McDonald, K.C., 2012, Satellite passive microwave detection of North America start of season: Remote Sensing of Environment, v. 123, p. 324–333, doi: 10.1016/j.rse.2012.03.025.

Jönsson, P., and Eklundh, L., 2004, TIMESAT—a program for analyzing time-series of satellite sensor data: Computers & Geosciences, v. 30, no. 8, p. 833–845, doi: 10.1016/j.cageo.2004.05.006.

Karl, T.R., Gleason, B.E., Menne, M.J., McMahon, J.R., Heim Jr., R.R., Brewer, M.J., Kunkel, K.E., Arndt, D.S., Privette, J.L., Bates, J.J., Groisman, P.Y., and Easterling, D.R., 2012, U . S . Temperature and Drought : Recent Anomalies and Trends: Eos, Transactions American Geophysical Union, v. 93, no. 47, p. 2011–2013.

Kim, Y., Jackson, T., and Bindlish, R., 2012, Radar Vegetation Index for Estimating the Vegetation Water Content of Rice and Soybean: IEEE Geoscience and Remote Sensing Letters, v. 9, no. 4, p. 564–568.

Larson, K.M., Braun, J.J., Small, E.E., Zavorotny, V.U., Member, S., Gutmann, E.D., and Bilich, A.L., 2010, GPS Multipath and Its Relation to Near-Surface Soil Moisture Content: IEEE Jounral of Slected Topics in Applied Earth Observations and Remote Sensing,, p. 1–9.

Larson, K.M., Gutmann, E.D., Zavorotny, V.U., Braun, J.J., Williams, M.W., and Nievinski, F.G., 2009, Can we measure snow depth with GPS receivers?: Geophysical Research Letters, v. 36, no. 17, p. L17502, doi: 10.1029/2009GL039430.

Larson, K.M., and Nievinski, F.G., 2012, GPS snow sensing: results from the EarthScope Plate Boundary Observatory: GPS Solutions,, doi: 10.1007/s10291-012-0259-7.

Larson, K.M., Small, E.E., Gutmann, E.D., Bilich, A.L., Braun, J.J., and Zavorotny, V.U., 2008, Use of GPS receivers as a soil moisture network for water cycle studies: Geophysical Research Letters, v. 35, no. 24, p. L24405, doi: 10.1029/2008GL036013.

Lu, D., 2006, The potential and challenge of remote sensing based biomass estimation: International Journal of Remote Sensing, v. 27, no. 7, p. 1297–1328, doi: 10.1080/01431160500486732.

Mitchell, K., Lohmann, D., Houser, P., Wood, E., Schaake, J., Robock, A., Cosgrove, B., Sheffield, J., Duan, Q., Luo, L., Higgins, R., Pinker, R., Tarpley, J., Lettenmaier, D., et al., 2003, The Multi-institution North American Land Data Assimilation System (NLDAS): Utilizing multiple GCIP products and partners in a continental distributed hydrological modeling system: J. Geophysical Research- Atmosphere,.

Morisette, J.T., Richardson, A.D., Knapp, A.K., Fisher, J.I., Graham, E. a, Abatzoglou, J., Wilson, B.E., Breshears, D.D., Henebry, G.M., Hanes, J.M., and Liang, L., 2009, Tracking the rhythm of the seasons in the face of global change: phenological research in the 21st century: Frontiers in Ecology and the Environment, v. 7, no. 5, p. 253–260, doi: 10.1890/070217.

Murai, S., 1993, Remote Sensing Note, *in* Japan Assoication on Remote Sensing, p. 56–96.

Myneni, R.B., and Williams, D.L., 1994, On the Relationship between FAPAR and NDVI: Remote Sensing of Environment, v. 211, no. April, p. 200–211.

Nemani, R.R., Keeling, C.D., Hashimoto, H., Jolly, W.M., Piper, S.C., Tucker, C.J., Myneni, R.B., and Running, S.W., 2003, Climate-driven increases in global terrestrial net primary production from 1982 to 1999.: Science, v. 300, no. 5625, p. 1560–3, doi: 10.1126/science.1082750.

Omernik, J.M., 1987, Ecoregions of the Conterminous United States: Annals of th Association of American Geographers, v. 77, no. 1, p. 118–125.

O'Neill, P.E., Jackson, T.J., Blanchard, B.J., Wang, J.R., and Gould, W.I., 1984, Effects of corn stalk orientation and water content on passive microwave sensing of soil moisture: Remote Sensing of Environment, v. 16, no. 1, p. 55–67, doi: 10.1016/0034-4257(84)90027-0.

Parmesan, C., 2007, Influences of species, latitudes and methodologies on estimates of phenological response to global warming: Global Change Biology, v. 13, no. 9, p. 1860–1872, doi: 10.1111/j.1365-2486.2007.01404.x.

Paruelo, J., and Aguiar, M., 1993, Environmental controls of NDVI dynamics in Patagonia based on NOAA-AVHRR satellite data: Journal of Vegetation Science, v. 4, p. 425–428.

Paruelo, J., Epstein, H., Lauenroth, W., and Burke, I., 1997, ANPP estimates from NDVI for the central grassland region of the United States: Ecology, v. 78, no. 3, p. 953–958.

Paruelo, J., and Lauenroth, W., 1995, Regional patterns of normalized difference vegetation index in North American shrublands and grasslands: Ecology, v. 76, no. 6, p. 1888–1898.

Peñuelas, J., 2009, Phenology feedbacks on climate change: Science, v. 324, no. 5929, p. 887–8, doi: 10.1126/science.1173004.

Reed, Bradley C, Brown, Jesslyn F., VanderZee, Darrel, Lovelend, Thomas R., Merchant, James W., Ohlen, D.O., 1994, Measuring phenological variability from satellite imagery: Journal of Vegetation Science, v. 5, p. 703–714.

Rodriguez-Alvarez, N., Bosch-Lluis, X., Camps, A., Aguasca, A., Vall-llossera, M., Valencia, E., Ramos-Perez, I., and Park, H., 2011, Review of crop growth and soil moisture monitoring from a ground-based instrument implementing the Interference Pattern GNSS-R Technique: Radio Science, v. 46, p. RS0C03, doi: 10.1029/2011RS004680.

Rodriguez-Iturbe, I., 2000, Ecohydrology : A hydrologic perspective of climate-soil-vegetation dynamics: Water Resources Research, v. 36, no. 1, p. 3–9.

Rondeaux, G., Steven, M., and Baret, F., 1996, Optimization of Soil-Adjusted Vegetation Indices: Remote Sensing of Environment, v. 107, no. August 1994, p. 95–107.

De Roo, R.D., Ulaby, F.T., and Dobson, M.C., 2001, A semi-empirical backscattering model at L-band and C-band for a soybean canopy with soil moisture inversion: IEEE Transactions on Geoscience and Remote Sensing, v. 39, no. 4, p. 864–872, doi: 10.1109/36.917912.

Running, S.W., and Nemani, R.R., 1988, Relating seasonal patterns of the AVHRR vegetation index to simulated photosynthesis and transpiration of forests in different climates: Remote Sensing of Environment, v. 24, p. 347–367.

Schmugge, T., 1978, Remote sensing of surface soil moisture.: Journal of Applied Meteorology, v. 17, p. 1549–1557.

Schwartz, M.D., Ahas, R., and Aasa, A., 2006, Onset of spring starting earlier across the Northern Hemisphere: Global Change Biology, v. 12, no. 2, p. 343–351, doi: 10.1111/j.1365-2486.2005.01097.x.

Sellers, P.J., Berry, J. A., Collatz, G.J., Field, C.B., and Hall, F.G., 1992, Canopy reflectance, photosynthesis, and transpiration. III. A reanalysis using improved leaf models and a new canopy integration scheme.: Remote Sensing of Environment, v. 42, no. 3, p. 187–216, doi: 10.1016/0034-4257(92)90102-P.

Sellers, P., Heiser, M., and Hall, F., 1995, Effects of spatial variability in topography, vegetation cover and soil moisture on area-averaged surface fluxes: A case study using the FIFE 1989 data: Journal of Geophysical Research, v. 100, no. 95.

Small, E.E., Larson, K.M., and Braun, J.J., 2010, Sensing vegetation growth with reflected GPS signals: Geophysical Research Letters, v. 37, no. 12, p. L12401, doi: 10.1029/2010GL042951.

Swets, D.L., College, A., Ave, S.S., and Falls, S., 2001, A Weighted Least-Squares Approach to Temporal NDVI Smoothing: , no. Figure 1.

Tarpley, J.D., Schneider, S.R., and Money, R.L., 1984, Global Vegetation Indices from the NOAA-7 Meteorological Satellite: Journal of Climate and Applied Meterology, v. 23, p. 491–494.

U.S. Environmental Protection Agency, 2011, Landscape and Predictive Tools: A Guide to Spatial Analysis for Environmental Assessment:, EPA/100/R–11/002 p.

Ulaby, F., Allen, C., Eger, G., and Kanemasu, E., 1984, Relating the microwave backscattering coefficient to leaf area index: Remote Sensing of Environment.

Ulaby, F., and Wilson, E., 1985, Microwave attenuation properties of vegetation canopies: IEEE Transactions on Geoscience and Remote Sensing, , no. 5, p. 746–753.

Wang, J., Rich, P.M., and Price, K.P., 2003, Temporal responses of NDVI to precipitation and temperature in the central Great Plains, USA: International Journal of Remote Sensing, v. 24, no. 11, p. 2345–2364, doi: 10.1080/01431160210154812.

Wells, D., Beck, N., Delikaraoglou, D., Kleusberg, A., Krakiwsky, E., Lachapelle, G., Langley, R., Nakiboglu, M., Schwarz, K., Tranquillia, J., and Vanicek, P., 1999, Guide to GPS positioning.

White, M.A., 2005, A global framework for monitoring phenological responses to climate change: Geophysical Research Letters, v. 32, no. 4, p. 2–5, doi: 10.1029/2004GL021961.

White, M. A., De Beurs, K.M., Didan, K., Inouye, D.W., Richardson, A.D., Jensen, O.P., O'Keefe, J., Zhang, G., Nemani, R.R., Van Leeuwen, W.J.D., Brown, J.F., De Wit, A., Schaepman, M., Lin, X., et al., 2009, Intercomparison, interpretation, and assessment of spring phenology in North America estimated from remote sensing for 1982-2006: Global Change Biology, v. 15, no. 10, p. 2335–2359, doi: 10.1111/j.1365-2486.2009.01910.x.

Wigneron, J., Ferrazzoli, P., Olioso, A., Bertuzzi, P., and Chanzy, A., 1997, A Simple Approach To Monitor Crop Biomass from C-Band Radar Data: Remote Sensing of Environment, v. 4257, no. 99, p. 179–188.

Wiken, E., Nava, F.J., and Jimen, G.G., 2011, North American Terrestrial Ecoregions—Level III. Commission for Environmental Cooperation, Montreal, Canada:.

Wolfe, D.W., Schwartz, M.D., and Lakso, A.N., 2005, Climate change and shifts in spring phenology of three horticultural woody perennials in northeastern USA: International Journal of Biometeorol, v. 49, p. 303–309, doi: 10.1007/s00484-004-0248-9.